AIAA JOURNAL
Vol. 55, No. 11, November 2017

Flux-Line Theory: A Novel Analytical Model for Cycloturbines

Zachary Adams* and Jun Chen†
Purdue University, West Lafayette, Indiana 47907

DOI: 10.2514/1.J055804

In this paper, a novel low-order blade element momentum model, called flux-line theory, is developed for predicting the performance of cycloturbines (variable-pitch vertical-axis wind turbines). It improves upon prior momentum theories by capturing flow expansion/contraction and bending through the turbine. This is accomplished by performing fluid calculations in a coordinate system fixed to streamlines for which the spatial locations are not predescribed. A transformation determines the Cartesian location of streamlines through the rotor disk, and additional calculations determine the power and forces produced. Validations against three sets of experimental data demonstrate improvement over other existing streamtube models. An extension of the theory removes dependence on a blade element model to better understand how turbine–fluid interaction impacts power production. A numerical optimization and simplified analytical analysis identify that maximum power (for a turbine that exclusively decelerates the flow) is produced when the upstream portion of the rotor does not interact with the flow, whereas the downstream portion of the turbine decelerates the flow by just over one-third of the freestream value. The theoretical power coefficient limit falls in a range below 0.8, depending on the prescription of the submodel describing the angle at which the flow crosses the blade path (0.597 for the best-fit model). A larger effective turbine area explains the higher-than-Betz limit result.

Nomenclature

A_{e_d}	=	effective area of downstream flux line
A_{e_u}	=	effective area of upstream flux line
A_{fluxline}	=	circumferential area of a flux line within an analysis control volume
$A_{\text{projected}}$	=	rectangular projected area of the rotor ($2br$)
$A_{\text{streamtube}}$	=	cross-sectional area of an analysis streamtube
A_∞	=	freestream area of flow that proceeds through the rotor
a_d	=	downstream flux-line interference factor
a_u	=	upstream flux-line interference factor
b	=	rotor span
C_d	=	section drag coefficient
C_l	=	section lift coefficient
C_m	=	section moment coefficient
C_p	=	coefficient of power
$F_\parallel$	=	force the streamtube exerts on the blade parallel to streamline
$F_\perp$	=	force the streamtube exerts on the blade perpendicular to streamline
f_x	=	x component of force
f_y	=	y component of force
$f_\parallel$	=	force per unit area flux line that streamtube exerts on blade that is parallel to streamline
$f_\perp$	=	force per unit area flux line that streamtube exerts on blade perpendicular to streamline
$\dot{m}$	=	mass flux
n	=	number of blades
P	=	turbine/rotor power
P_∞	=	freestream static pressure
r	=	rotor radius
s	=	streamline index
V_a	=	induced velocity
V_d	=	induced velocity through the downstream flux line/rotor
V_r	=	flow velocity relative to blade
V_u	=	induced velocity through the upstream flux line/rotor
$V_{u_{\text{wake}}}$	=	freestream pressure velocity between the upstream and downstream flux lines
V_w	=	wake velocity
V_x	=	x component of velocity
V_y	=	y component of velocity
V_∞	=	freestream velocity
x	=	Cartesian coordinate parallel to the direction of freestream flow
y	=	Cartesian coordinate perpendicular to the direction of freestream flow
y_w	=	Cartesian wake coordinate of a streamline
y_∞	=	Cartesian freestream coordinate of a streamline
α	=	blade angle of attack
β	=	angle between flow velocity relative to blade and tangent to rotor
γ	=	angle between rotor flux line and streamline
ϵ	=	two-parameter modeling variable describing flow expansion/contraction
ζ	=	angle between streamline and flow velocity relative to blade
η	=	two-parameter modeling variable describing fluid bending
θ	=	blade pitch
θ_x	=	angle between a streamline and the x axis, measured positive counterclockwise
λ	=	tip speed ratio
ρ	=	fluid density
σ	=	rotor solidity
ϕ	=	azimuth/cyclic position around the rotor
Ω	=	rotational speed

Received 28 October 2016; revision received 2 May 2017; accepted for publication 10 May 2017; published online 31 July 2017.

*School of Mechanical Engineering; adams31@purdue.edu.
†Associate Professor, School of Mechanical Engineering; junchen@purdue.edu.

I. Introduction

VERTICAL-AXIS wind turbines (VAWTs) are an established alternative to the widespread horizontal-axis wind turbines (HAWTs) with immense potential for expanding renewable power generation to unexplored locations. VAWTs harvest wind energy via aerodynamic forces applied on the blades for which the axis of rotation is perpendicular to the incoming wind. This definition encompasses a wide range of lift-type and drag-type VAWTs. Of the lift-type VAWTs, the H-bar type shown in Fig. 1 represents the simplest model for analysis. When its blades are oscillated relative to the rotating structure during operation, the concept is known as

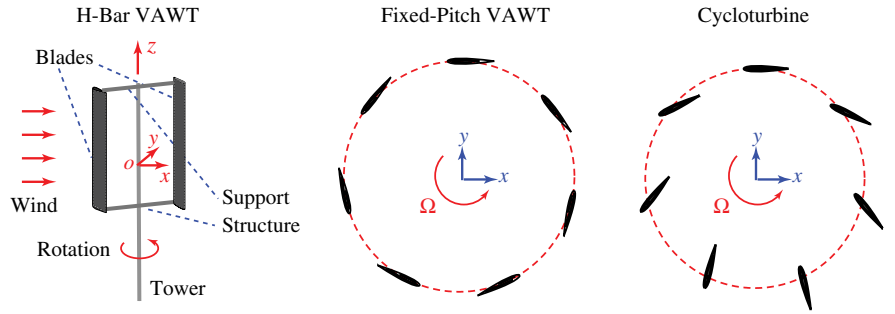

Fig. 1 Schematics of H-bar-type VAWT and comparisons of fixed-pitch and cycloturbine (variable-pitch) variants.

cycloturbine. The optimal design of the blade pitch scheme of cycloturbines leads to an increased power efficiency when compared to the traditional fixed-pitch VAWTs.

VAWTs can generate more power per unit land area than HAWTs by simply increasing their blade length and keeping an unchanged blade swept land area [1,2]. This power density may be further boosted in dynamic conditions where rapidly shifting wind direction attenuates the performance of HAWTs [3]. VAWTs are also promising for offshore applications without rigid and expensive sea floor anchoring because the generator, gearbox, and electronics can be positioned at the base of a floating platform. This placement lowers the turbine center of gravity with increased stability and eases access for installation and maintenance [4,5].

Despite these and other advantages, VAWTs have not been widely implemented. In part, this is because most VAWTs use fixed-pitch blades; so, they are not self-starting and suffer from low aerodynamic efficiency. Fixed-pitch VAWT blades often operate at angles of attack that either prevent power extraction or stall the blade during some portion of their revolution. These counterproductive aerodynamic forces attenuate available turbine power and cause damaging oscillatory loads [1,6,7]. Such blade pitch angles often prohibit operation at low rotational speeds, and most fixed-pitch lift*based VAWTs must be accelerated by a driving mechanism (e.g., motor) to pass that region of negative power. Cycloturbines overcome this difficulty by adjusting the blades to account for the relative flow direction, which makes them more efficient and self-starting. However, the proper selection of blade dynamics is nontrivial.

Because the axis of a VAWT is perpendicular to the incoming wind, the blades continuously transverse different flow conditions. The relative flow direction and magnitude experienced by the blade are primarily determined by the tip-speed ratio (TSR): $\lambda = \Omega r/U$, where U is the wind speed, r is the rotor radius, and Ω is the angular velocity of blade rotation. Figure 2 shows a VAWT blade pitched for a zero-degree angle of attack at various TSRs. Those less than unity ($\lambda < 1$) are referred to as curtate TSRs, and the relative wind experienced by the blade is angled within 90 deg of the freestream flow. At higher prolate TSRs ($\lambda > 1$), the relative blade wind velocity is angled within 90 deg of the blade trajectory. A cycloid TSR ($\lambda = 1$) includes a point where the velocity of the retreating blade is exactly matched by the forward flow velocity. To achieve optimum efficiency, VAWTs must account for these diverse flow directions, which are further complicated by the interaction between the turbine and the flowfield.

Historically, researchers have developed a spectrum of models for predicting the VAWT performance, including a variety of streamtube models, vortex simulations [8–14], and computational fluid dynamics (CFD) simulations [1,15–18]. Although CFD simulations and vortex methods have proven quantitatively accurate [1,8,9,15,16], they are computationally expensive and cannot distill VAWT performance into easy-to-implement low-order models that highlight the contribution and interaction of individual factors (i.e., blade pitch function, turbine solidity, and TSR). Streamtube models can provide such analytical insight, and their computational expense is negligible. They were adapted from

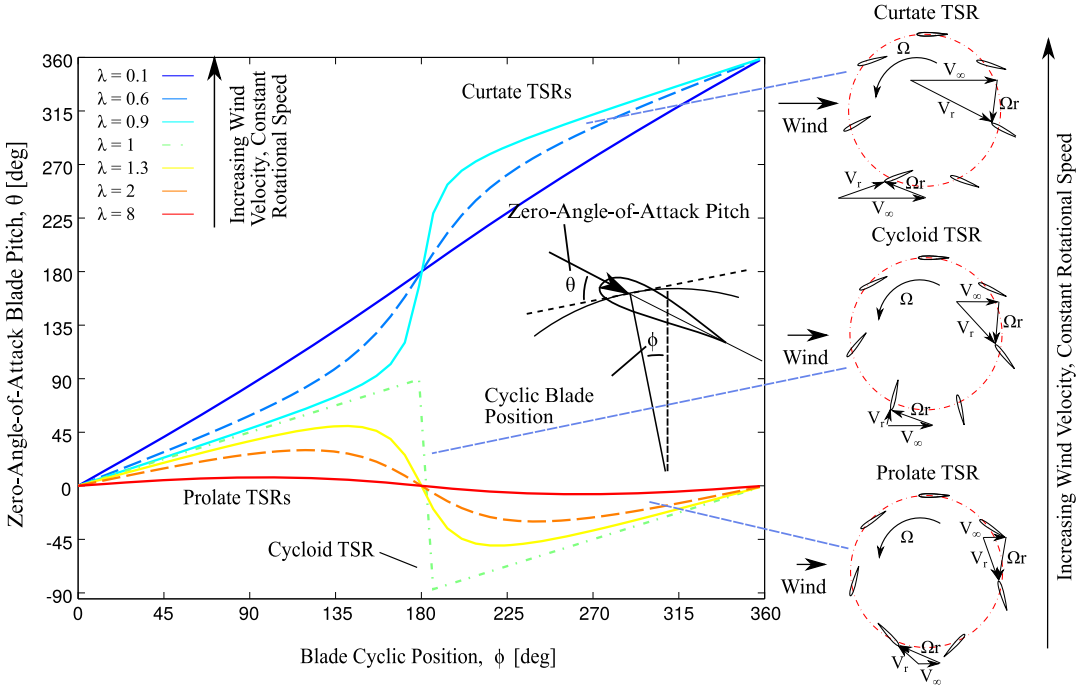

Fig. 2 Blade pitch required to achieve a 0 deg angle of attack as it rotates about the axis of a VAWT at various TSRs.

momentum models for HAWTs and propellers, which provide substantial insight into flow physics and are widely employed with ideal accuracy. However, streamtube models require improvement to properly account for flow expansion and curvature through VAWTs, which is the focus of the present paper.

Streamtube models apply the Glauert momentum theory to estimate the turbine–fluid interactions and to predict the relative blade velocity. In 1974, Templin proposed that the finite volume enclosed by the VAWT blades could be treated as the actuator disk in momentum theory [19]. In this single streamtube (SS) model (Fig. 3a), the freestream wind velocity V_∞ is slowed to an induced velocity V_a, which is assumed constant through the actuator disk. Because only the resultant equations of momentum theory are applied, the velocity through the rotor is calculated without accounting for necessary variations in the streamtube area. Consequently, streamtube models are a freestream flow correction rather than a mathematically accurate simplification. Templin's model describes the overall trends of the VAWT performance but overestimates the extracted wind power [10,19]. Noll and Ham later improved the streamtube model by accounting for strut drag and dynamic blade stall in their 1980 cycloturbine model.

To account for turbine–fluid variation across the turbine, Wilson and Lissaman later proposed the multiple streamtube (MS) model [22], which divides the rotor disk into several parallel streamtubes (Fig. 3b) and calculates the induced velocity based on the lift force on the blades through both the upstream and downstream segments. Strickland et al. further improved the model by including blade drag in the momentum exchange computation [12]. Paraschivoiu distinguished the upstream and downstream segments of the rotor with the double multiple streamtube (DMS) theory in 1981 [20]. Each of the multiple streamtubes is analyzed as a pair of actuator disks in tandem (Fig. 3c). The flow accepted by the second actuator disk is the wake flow from the first idealized rotor which Paraschivoiu found to closely match the experimental data [20,21].

Although increasing the points at which the induced velocity is calculated increases model fidelity, the aforementioned streamtube models fundamentally ignores that the turbine alters both the direction and magnitude of the flowfield. Read and Sharpe (1977) introduced a multiple streamtube model, where the angle of the streamtube lines varied to model the increasing streamtube size [23]. They computed the induced velocity based on a combined mass momentum approach. This increased the model predictive accuracy of blade forces throughout the cycle in comparison to the basic multiple streamtube model but with an underpredicted net power [23]. More recently, Soraghan et al. combined the linear expansion multiple streamtube and double multiple streamtube models (Fig. 3d) [24]. They implemented a blade force prediction algorithm pioneered by Larsen et al. [25] to account for dynamic stall and flow curvature. This model predicts the turbine power for $\lambda > 2.5$ on lightly loaded turbines within 5% but overpredicts the power at $1.5 < \lambda < 2.5$ [25]. Dyachuk et al. (2014) implemented the same linear expansion DMS model to compare the performance of Leishman–Beddoes and Gormont unsteady blade aerodynamics models on VAWTs [26]. Although they found Leishman–Beddoes to outperform Gormont, neither consistently matched the experimental data; and the accuracy of the linear expansion DMS model was unclear [26].

The key disadvantage of the existing streamtube models is they simply correct for wind speed rather than actually computing the flowpath through the rotor. In reality, flow expansion and bending before and within the turbine alter the relative angle of attack of the blades [1]. Because the blade forces are extremely sensitive to the relative flow angle, it is essential to provide an accurate estimation of the local flow velocity vector for accurate modeling of the overall performance. In this paper, we propose a novel flux-line theory, which provides a blade element momentum model to estimate the performance of VAWTs and a pure momentum model to identify theoretical system limitations. The new model identifies fundamental VAWT physics to include a system performance ceiling similar to the Betz limit for HAWTs. Although the present work emphasizes the application of flux-line theory to VAWTs, it can also be applied to model cyclorotors in hover and forward flight, which will be addressed in separate publications.

In this paper, Sec. II describes the physical model, adopted assumptions, and mathematics behind the blade element momentum variant of the theory. Next, Sec. III validates this model against three sets of experimental data. Section IV extends flux-line theory by eliminating dependence on the blade element model, which enables determination of the maximum theoretical power limit. Finally, Sec. V gives a summary and outlook.

II. Framework of Flux-Line Theory

A. Physical Model and Assumptions

The flux-line theory is developed by adopting the following assumptions: 1) incompressible and inviscid flow; 2) two-dimensional flow, with no variation along the z direction; 3) neglected gravity; 4) quasi-steady flow (effectively, an infinite number of blades); and 5) the rotor disk steadily imparting a discrete momentum change (both magnitude and direction) to the fluid at every cyclic position. To implement this new model, as shown in Fig. 4, flow through the rotor disk is sectioned by four newly defined "flux lines": a freestream flux line perpendicular to the undisturbed freestream flow, an upstream flux line corresponding to the upstream portion of the rotor circle where wind initially enters the rotor disk, a downstream flux line corresponding to the downstream portion of the same circle where the wind exits the rotor disk, and a wake flux line crossing the flow in the far wake. The theory is named because the analyses are performed on each flux line.

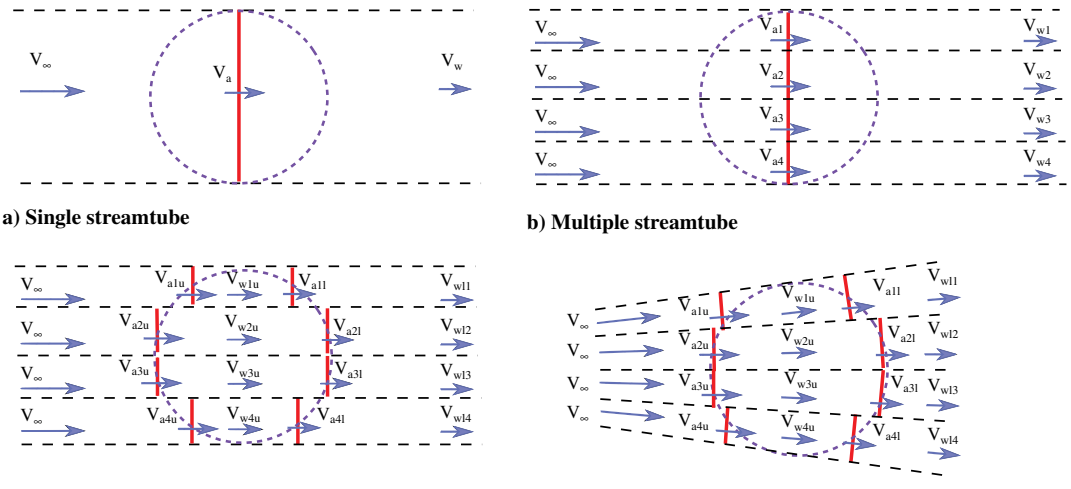

a) Single streamtube

b) Multiple streamtube

c) Double multiple streamtube

d) Double multiple streamtube with linear expansion

Fig. 3 Streamtube model variations.

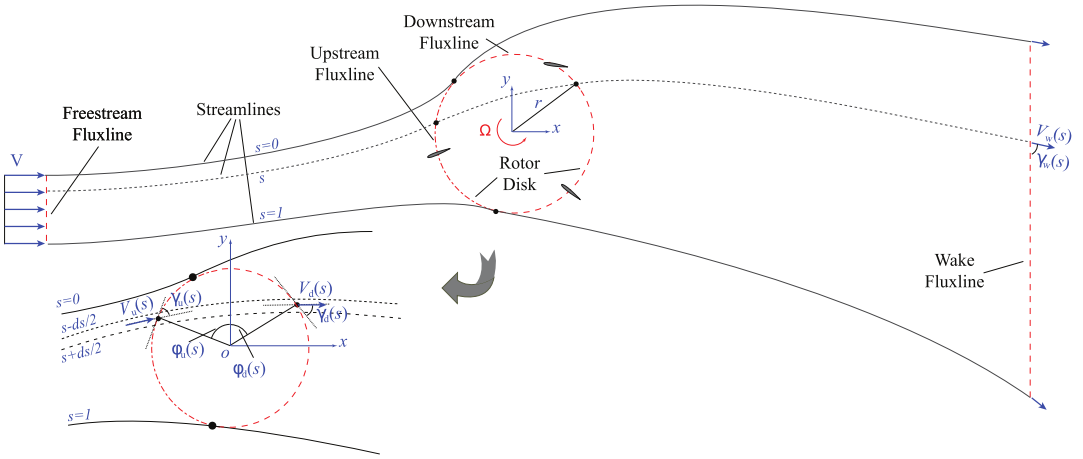

Fig. 4 Schematic of flux-line model: system, geometry, and variables.

Each flux line can be labeled in a Cartesian system (by the three-dimensional coordinates x–y–z) and a streamline system, respectively. In the streamline system, a streamline index s is assigned to each streamline within the domain, where all points on a specific streamline are labeled by a consistent s $(0 \le s \le 1)$. The two marginal streamlines, $s = 0$ and $s = 1$, are tangent to the rotor disk. Flow parameters (induced velocity, flow angle, forces, etc.) can be described as either a function of the streamline position $f(s)$ or their Cartesian location $f(x, y)/f(\phi)$. In the following analysis, subscripts ∞, u, d, and w, denote parameters at the freestream flux line, the upstream flux line, the downstream flux line, and the wake flux line, respectively. The flux-line crossing angle γ is spanned by the streamline and flux line at their intersection (Fig. 4). By this definition, $\gamma_\infty = \pi/2, 0 \le \gamma_u, \gamma_d \le \pi$ as s increases from zero to one, and γ_w holds a constant value between zero and π.

B. Mathematics Describing Flow Physics

1. *Conservation of Mass*

A streamline s and its adjacent neighborhood

$$s - \frac{ds}{2} < s < s + \frac{ds}{2}$$

span a two-dimensional streamtube (inset of Fig. 4) with conserved mass flux at every cross section, i.e.,

$$\begin{aligned} V_\infty A_\infty^{(s-(ds/2)\to s+(ds/2))} &= V_u(s) A_u^{(s-(ds/2)\to s+(ds/2))} \\ &= V_d(s) A_d^{(s-(ds/2)\to s+(ds/2))} \\ &= V_w(s) A_w^{(s-(ds/2)\to s+(ds/2))} \end{aligned} \tag{1}$$

where A denotes the effective cross-sectional area of the streamtube. Considering unit depth along the z direction, the area is related to the flux-line coordinates of the two streamlines. Thus, from Eq. (1), one has

$$\begin{aligned} & V_\infty \left[y_\infty\left(s + \frac{ds}{2}\right) - y_\infty\left(s - \frac{ds}{2}\right) \right] \\ &= V_u(s) r \left[\phi_u\left(s + \frac{ds}{2}\right) - \phi_u\left(s - \frac{ds}{2}\right) \right] \sin(\gamma_u(s)) \\ &= V_d(s) r \left[\phi_d\left(s + \frac{ds}{2}\right) - \phi_d\left(s - \frac{ds}{2}\right) \right] \sin(\gamma_d(s)) \\ &= V_w(s) \left[y_w\left(s + \frac{ds}{2}\right) - y_w\left(s - \frac{ds}{2}\right) \right] \end{aligned} \tag{2}$$

where y_∞ and y_w represent the y intercepts of the streamlines with freestream and wake flux lines, respectively; and r is the radius of the rotor disk. Applying a first-order Taylor's expansion yields

$$\begin{aligned} V_\infty \frac{dy_\infty}{ds} &= V_u(s) r \frac{d\phi_u}{ds} \sin(\gamma_u(s)) = V_d(s) r \frac{d\phi_d}{ds} \sin(\gamma_d(s)) \\ &= V_w(s) \frac{dy_w}{ds} \end{aligned} \tag{3}$$

2. *Conservation of Momentum*

As the flow passes through the rotor disk, the interaction between the flow and the blades induces a momentum change (or force), extracted from or imparted to the fluid by rotating blades. This interaction is modeled by assuming that only the force component parallel to the streamline $F_\parallel$ contributes to this momentum (and velocity) change, as will be detailed later. This permits direct computation of the induced flow velocities from the blade forces. Those velocities are combined with data of all the streamline forces (including the perpendicular component $F_\perp$) to compute the directions at which the streamline s enters and exits the rotor disk, i.e., angles $\gamma_u(s)$ and $\gamma_d(s)$.

The Glauert actuator disk theory [27], commonly applied to propellers and HAWTs, is adopted in flux-line theory along each streamline by assuming that an instantaneous static pressure change occurs as flow passes through the actuator disk. At the entrance and exit of the control volume, the pressure equalizes to P_∞. The thrust or drag applied on the actuator disk is equivalent to the change in momentum:

$$T = \dot{m}(V_\infty - V_w) = \rho A V_a (V_\infty - V_w) \tag{4}$$

where V_a is the induced velocity across the actuator disk. T should also balance the pressure drop across the actuator disk:

$$T = A(P_u - P_d) \tag{5}$$

The Bernoulli equation relates the thrust and velocity of the far wake:

$$T = \frac{1}{2} \rho A (V_\infty^2 - V_w^2) \tag{6}$$

Combining Eqs. (4) and (6) gives

$$V_a = \frac{1}{2}(V_\infty + V_w) \tag{7}$$

The same analysis is applied to predict induced velocities at the upstream and downstream flux lines. When the pressure is assumed to restore to P_∞ inside the rotor disk, similar to Eq. (7), one gets

$$V_u(s) = \frac{1}{2}\left(V_\infty(s) + V_{u_{\text{wake}}}(s)\right) \tag{8}$$

and

$$V_d(s) = \frac{1}{2}\left(V_{u_{\text{wake}}}(s) + V_w(s)\right) \tag{9}$$

where $V_{u_{\text{wake}}}$ is the flow velocity inside the rotor disk along the streamline s. $V_{u_{\text{wake}}}$ can be determined by a control volume analysis, as shown in Fig. 5. As previously mentioned, $F_\parallel$ is assumed to only change the velocity magnitude; thus, the control volume is effectively linearly transformed (inset of Fig. 5), i.e.,

$$F_{\parallel u} = \dot{m}\left(V_\infty - V_{u_{\text{wake}}}\right) \tag{10}$$

The mass flow rate $\dot{m}$ is the product of the density, velocity, and cross-sectional area. Thus,

$$F_{\parallel u} = \rho V_u A_{\text{streamtube}}\left(V_\infty - V_{u_{\text{wake}}}\right) \tag{11}$$

Rearranging Eq. (11) yields

$$V_{u_{\text{wake}}} = V_\infty - \frac{F_{\parallel u}}{\rho A_{\text{streamtube}} V_u} \tag{12}$$

The streamtube area is related to the flux-line area by

$$A_{\text{streamtube}} = A_{\text{fluxline}} \sin\gamma \tag{13}$$

When considering an infinitesimal streamtube, it is convenient to consider the force per unit area flux line: $f_{\parallel u} = F_{\parallel u}/A_{\text{fluxline}}$. Substituting this expression into Eq. (12) yields

$$V_{u_{\text{wake}}} = V_\infty - \frac{f_{\parallel u}}{\rho V_u \sin\gamma_u} \tag{14}$$

Substituting Eq. (14) into Eq. (8) eliminates the dependence on the wake velocity:

$$V_u = V_\infty - \frac{f_{\parallel u}}{2\rho V_u \sin\gamma_u} \tag{15}$$

Rearranging provides a quadratic equation:

$$V_u^2 - V_u V_\infty + \frac{f_{\parallel u}}{2\rho \sin\gamma_u} = 0 \tag{16}$$

where the only valid solution is

$$V_u(s) = \frac{V_\infty(s)}{2} + \sqrt{\frac{V_\infty^2(s)}{4} - \frac{f_{\parallel u}(s)}{2\rho \sin\gamma_u}} \tag{17}$$

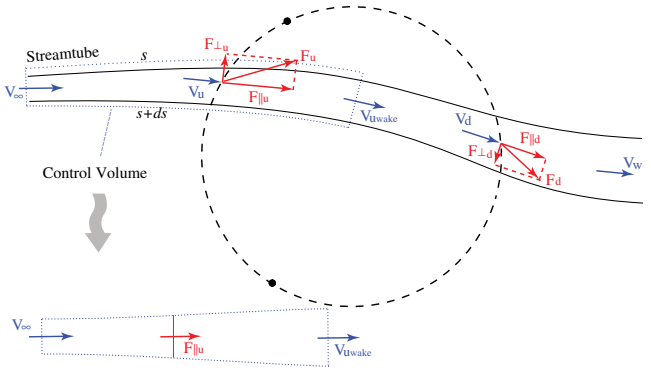

Fig. 5 Streamtube, associated forces, and control volume for upper flux-line analysis.

The downstream flux-line induced velocity and wake velocity can be similarly derived. By conservation of momentum,

$$\dot{m}\left(V_{u_{\text{wake}}} - V_w\right) = F_{\parallel d} \tag{18}$$

Rearranging gives the wake velocity

$$V_w = V_{u_{\text{wake}}} - \frac{f_{\parallel d}}{\rho V_d \sin\gamma_d} \tag{19}$$

Substituting into Eq. (9) and rearranging gives

$$V_d^2 - V_d V_{u_{\text{wake}}} + \frac{f_{\parallel d}}{2\rho \sin\gamma_d} = 0 \tag{20}$$

with the solution

$$V_d(s) = \frac{V_{u_{\text{wake}}}(s)}{2} + \sqrt{\frac{V_{u_{\text{wake}}}^2(s)}{4} - \frac{f_{\parallel d}(s)}{2\rho \sin\gamma_d}} \tag{21}$$

Given the force [$f_{\parallel u}(s)$ and $f_{\parallel d}(s)$] and angular [$\gamma_u(s)$ and $\gamma_d(s)$] distributions, Eqs. (17) and (21) predict the flux-line velocities at streamline s without reference to the geometry of the system. This powerful result provides rapid calculation of rotor inflow. Once the velocity is determined, the angle at which each streamline crosses the flux lines can be determined as explained in the following section.

3. *Determining Flow Angles Across Each Flux line*

To globally model the streamline bending through the rotor disk, we propose a two-parameter model to describe $\gamma_u(s)$ and $\gamma_d(s)$.

4. *Determining Flow Angles Across Each Fluxline: The Two Parameter γ Model*

The model functions for γ_u and γ_d must satisfy the following properties:

1) $\gamma_u(s=0) = \gamma_d(s=0) = 0$.
2) $\gamma_u(s=1) = \gamma_d(s=1) = \pi$.
3) If the turbine does not produce any forces (no disturbance to the incoming flow), the flow through rotor keeps uniform along the x direction, leading to $\gamma_u(s) = \gamma_d(s) = \arccos(1–2s)$.
4) As the drag of the turbine increases, less flow proceeds through the turbine. Increasing the drag causes the flow to resemble that of the flow around a circular cylinder. Consequently, at a high enough drag, the distribution must converge toward a stagnation point distribution:

$$\gamma_u(s) = \gamma_d(s) = \begin{cases} 0 & \text{when} \quad 0 \le s \le \dfrac{1}{2} \\ \pi & \text{when} \quad \dfrac{1}{2} < s \le 1 \end{cases} \tag{22}$$

5) If the system is driven as a propeller with a large thrust, then the flow will curve into the circular rotor akin to flow in a bell-mouth engine inlet. Ultimately, a sufficiently large thrust should produce a distribution where the flow everywhere is perpendicular to the upstream flux line. Mathematically, $\gamma_u(s) = \pi/2$ in this case for $0 \le s \le 1$.
6) The distributions must be continuous and differentiable.

We propose the following two-parameter ($\epsilon - \eta$) models that meet these requirements:

$$\gamma_u(s) = \arctan\left(\frac{2\sqrt{s^{\eta_u}(1-s^{\eta_u})}}{\epsilon_u(1–2s^{\eta_u})}\right) \tag{23}$$

and

$$\gamma_d(s) = \arctan\left(\frac{2\sqrt{s^{\eta_d}(1-s^{\eta_d})}}{\epsilon_d(1–2s^{\eta_d})}\right) \tag{24}$$

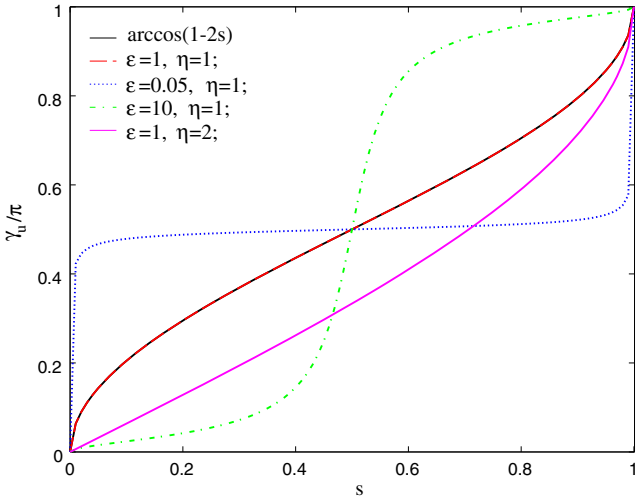

Fig. 6 Comparison of two-parameter distribution with inverse cosine distribution for various coefficients.

As shown in Fig. 6, $\gamma_u(s)$ and $\gamma_d(s)$ equate to $\arccos(1-2s)$ when $\epsilon_u = \epsilon_d = 1$ and $\eta_u = \eta_d = 1$. Figure 6 also compares various predictions of $\gamma_u(s)$ with different combinations of ϵ and η. Increasing ϵ_u (or ϵ_d) forms the distribution toward a stagnation point distribution, whereas decreasing it nearer to zero molds the distributions toward $\gamma_u(s) = \pi/2$. Note that ϵ_u and ϵ_d are constrained between zero and positive infinity. Changing the coefficients η_u (or η_d) alters the net skew of the wake. The mathematical limits of η_u are also between zero and positive infinity; however, only values near one are physically sensible.

The coefficients ϵ_u, ϵ_d, η_u, and η_d are determined by flow momentum balances on the upstream and downstream flux lines using a control volume analysis (Fig. 7) in the x direction

$$\int_0^1 \rho V_\infty \frac{\mathrm{d}y_\infty}{\mathrm{d}s} V_u \cos\theta_{xu}\,\mathrm{d}s - \int_0^1 \rho V_\infty^2 \frac{\mathrm{d}y_\infty}{\mathrm{d}s}\,\mathrm{d}s = \int_0^1 \frac{1}{2}\rho(V_\infty^2 - V_u^2)\sin\phi_u \frac{\mathrm{d}\phi_u}{\mathrm{d}s} r\,\mathrm{d}s \tag{25}$$

because

$$P_u(s) = P_\infty + \frac{1}{2}\rho(V_\infty^2 - V_u^2(s)) \tag{26}$$

and

$$\theta_{xu}(s) = \phi_u(s) - \gamma_u(s) \tag{27}$$

In the y direction,

$$\int_0^1 \rho V_\infty \frac{\mathrm{d}y_\infty}{\mathrm{d}s} V_u \sin\theta_{xu}\,\mathrm{d}s = \int_0^1 \frac{1}{2}\rho(V_\infty^2 - V_u^2)\cos\phi_u \frac{\mathrm{d}\phi_u}{\mathrm{d}s} r\,\mathrm{d}s \tag{28}$$

Equations (25) and (28) are numerically solved for ϵ_u and η_u. Similarly, from momentum balances on the downstream control volume, in the x direction,

$$\int_0^1 \rho V_\infty \frac{\mathrm{d}y_\infty}{\mathrm{d}s} V_d \cos\theta_{xd}\,\mathrm{d}s - \int_0^1 \rho V_\infty \frac{\mathrm{d}y_\infty}{\mathrm{d}s} V_u \cos\theta_{xu}\,\mathrm{d}s = \int_0^1 f_{ux}\frac{\mathrm{d}\phi_u}{\mathrm{d}s} r\,\mathrm{d}s + \int_0^1 P_u \sin\phi_u \frac{\mathrm{d}\phi_u}{\mathrm{d}s} r\,\mathrm{d}s - \int_0^1 P_d \sin\phi_d \frac{\mathrm{d}\phi_d}{\mathrm{d}s} r\,\mathrm{d}s \tag{29}$$

and, in the y direction,

$$\int_0^1 \rho V_\infty \frac{\mathrm{d}y_\infty}{\mathrm{d}s} V_d \sin\theta_{xd}\,\mathrm{d}s - \int_0^1 \rho V_\infty \frac{\mathrm{d}y_\infty}{\mathrm{d}s} V_u \sin\theta_{xu}\,\mathrm{d}s = \int_0^1 f_{uy}\frac{\mathrm{d}\phi_u}{\mathrm{d}s} r\,\mathrm{d}s - \int_0^1 P_d \cos\phi_d \frac{\mathrm{d}\phi_d}{\mathrm{d}s} r\,\mathrm{d}s - \int_0^1 P_u \cos\phi_u \frac{d\phi_u}{ds} r\,\mathrm{d}s \tag{30}$$

where

$$P_d(s) = P_\infty + \frac{1}{2}\rho\left(V_{u_{\text{wake}}}^2 - V_d^2(s)\right) \tag{31}$$

and

$$\theta_{xd}(s) = -\phi_d(s) + \gamma_d(s) \tag{32}$$

Equations (29) and (30) are numerically solved for ϵ_d and η_d.

C. Transformation to Cartesian Domain

The conservation laws determine the velocity, angles, and relative spacing of streamlines as functions of streamline index s. To yield forces and power, these parameters must be transformed back into the Cartesian domain. This transformation centers on ensuring that the upstream and downstream flux lines form a complete rotor disk, i.e.,

$$\int_0^1 \frac{\mathrm{d}\phi_u(s)}{\mathrm{d}s}\,\mathrm{d}s + \int_0^1 \frac{\mathrm{d}\phi_d(s)}{\mathrm{d}s}\,\mathrm{d}s = 2\pi \tag{33}$$

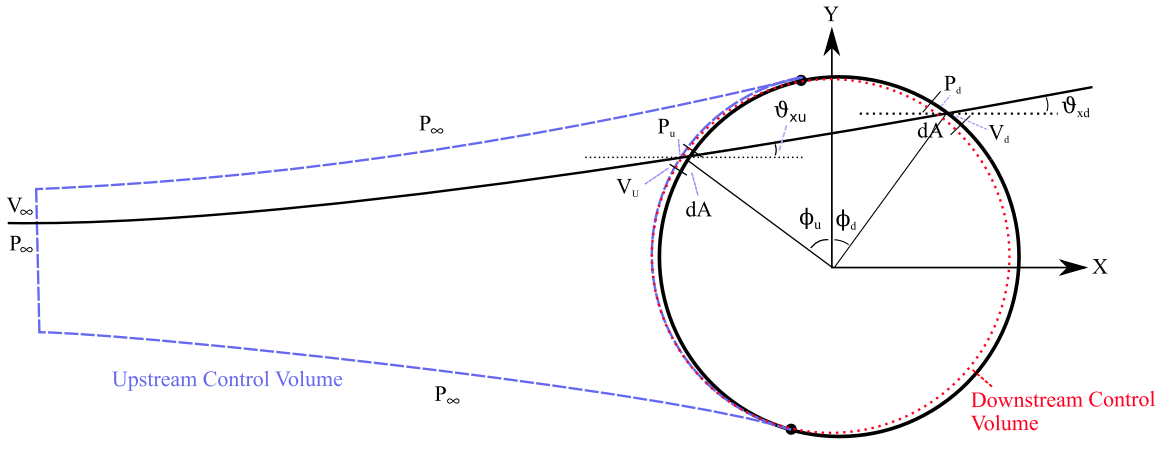

Fig. 7 Control volumes for upstream and downstream flux-line gamma distribution analyses.

Combining the conservation of mass [Eq. (3)] with Eq. (33) yields

$$\int_0^1 \frac{V_\infty}{V_u(s)\sin(\gamma_u(s))r}\frac{\mathrm{d}y_\infty}{\mathrm{d}s}\,\mathrm{d}s + \int_0^1 \frac{V_\infty}{V_d(s)\sin(\gamma_d(s))r}\frac{\mathrm{d}y_\infty}{\mathrm{d}s}\,\mathrm{d}s = 2\pi \tag{34}$$

Given the known force distributions from a blade element analysis, $\mathrm{d}y_\infty/\mathrm{d}s$ is the only unknown. Rearranging provides

$$\frac{1}{2r}\frac{\mathrm{d}y_\infty}{\mathrm{d}s} = \frac{\pi}{\int_0^1 (V_\infty/V_u(s)\sin(\gamma_u(s)))\mathrm{d}s + \int_0^1 (V_\infty/V_d(s)\sin(\gamma_d(s)))\mathrm{d}s} \tag{35}$$

The parameter $\mathrm{d}y_\infty/\mathrm{d}s$ holds special significance because it identifies the area of freestream flow that is processed by the rotor. Its nondimensional form is the freestream area ratio:

$$\frac{A_\infty}{A_{\text{projected}}} = \frac{1}{2r}\frac{\mathrm{d}y_\infty}{\mathrm{d}s} \tag{36}$$

which is the ratio of the projected rotor area to the freestream flow area that proceeds through the rotor. A value of one signifies that the freestream area is equal to the projected area of the rotor, whereas smaller or larger values correspond to equivalently changing areas (Fig. 8). If all portions of the turbine extract energy from the flow, the freestream wind area that is processed will be smaller than the turbine projected area due to flow expansion. In the extreme case of infinite drag, no flow will proceed through the rotor and the freestream area ratio will be zero. For cyclorotor operation, the freestream area will be larger from flow contraction before the rotor. For a hovering cyclorotor, the freestream area and the freestream area ratio will be infinite:

$$\frac{A_\infty}{A_{\text{projected}}} = \frac{1}{2r}\frac{\mathrm{d}y_\infty}{\mathrm{d}s} \begin{cases} = 0 & A_\infty = 0 & \text{(Cycloturbine with in finite drag)} \\ < 1 & A_\infty < A_{\text{projected}} & \text{(Cycloturbine)} \\ = 1 \quad \text{if} & A_\infty = A_{\text{projected}} & \text{(Zeroloading)} \\ > 1 & A_\infty > A_{\text{projected}} & \text{(Cyclorotor)} \\ = \infty & A_\infty = \infty & \text{(Cyclorotor in hover)} \end{cases} \tag{37}$$

Once $\mathrm{d}y_\infty/\mathrm{d}s$ is known, $\phi_u(s)$, $\phi_d(s)$, and $y_w(s)$ are determined by integrating Eq. (3):

$$\phi_u(s) = \int_0^s \frac{\mathrm{d}\phi_u(s)}{\mathrm{d}s}\,\mathrm{d}s + \phi_u(s=0) = \int_0^s \frac{V_\infty}{V_u(s)\sin(\gamma_u(s))r}\frac{\mathrm{d}y_\infty}{\mathrm{d}s}\,\mathrm{d}s + \phi_u(s=0) \tag{38}$$

$$\phi_d(s) = \int_0^s \frac{\mathrm{d}\phi_d(s)}{\mathrm{d}s}\,\mathrm{d}s + \phi_d(s=0) = \int_0^s \frac{V_\infty}{V_d(s)\sin(\gamma_u(s))r}\frac{\mathrm{d}y_\infty}{\mathrm{d}s}\,\mathrm{d}s + \phi_d(s=0) \tag{39}$$

$$y_w(s) = \int_0^s \frac{\mathrm{d}y_w(s)}{\mathrm{d}s}\,\mathrm{d}s + y_w(s=0) \tag{40}$$

D. Computation of Power and Forces

1. Blade Element Method

A blade element method is employed to determine $f_\parallel(s)$ and $f_\perp(s)$. The relative flow experienced by the blade is determined by the vector sum of the induced velocity and rotational velocity of the turbine blade. The magnitudes of these resultant velocities, as shown in Fig. 9, are

$$V_{r_u} = \sqrt{(\Omega r\cos\gamma_u + V_u)^2 + (\Omega r\sin\gamma_u)^2} \tag{41}$$

and

$$V_{r_d} = \sqrt{(\Omega r\cos\gamma_d + V_d)^2 + (\Omega r\sin\gamma_d)^2} \tag{42}$$

The directions can be specified by the angles between the resultant velocities and the streamline:

$$\zeta_u = \arctan\left(\frac{\Omega r\sin\gamma_u}{\Omega r\cos\gamma_u + V_u}\right) \tag{43}$$

$$\zeta_d = \arctan\left(\frac{\Omega r\sin\gamma_d}{\Omega r\cos\gamma_d + V_d}\right) \tag{44}$$

The angles ζ_u and ζ_d are also used to decompose the lift L and drag D into the components parallel and normal to the streamline.

Given the blade pitch angle θ_u or θ_d, the angles of attack can be determined:

$$\alpha_u = \theta_u - \gamma_u + \zeta_u \tag{45}$$

and

$$\alpha_d = \theta_d + \gamma_d - \zeta_u \tag{46}$$

Now, with the determined local velocity and angle of attack, the lift and drag forces on the blade can be determined by interpolation of experimental data (lift–drag characteristics), predictions of thin airfoil theory, or other methods. Advanced double multiple streamtube models used for VAWTs and cyclorotors model the

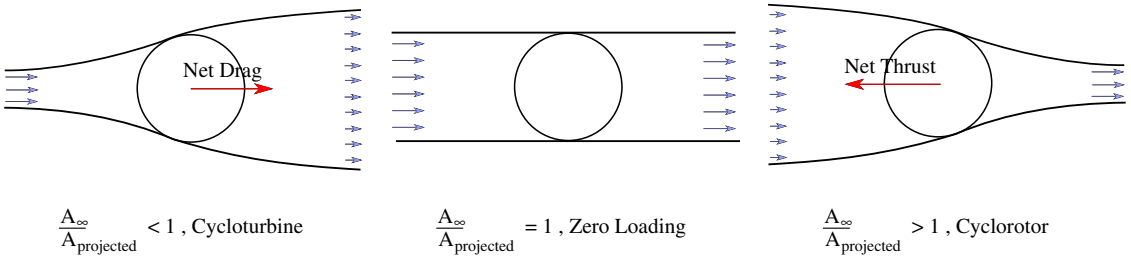

Fig. 8 Expansion or contraction of flow through the rotor, described by the freestream area ratio.

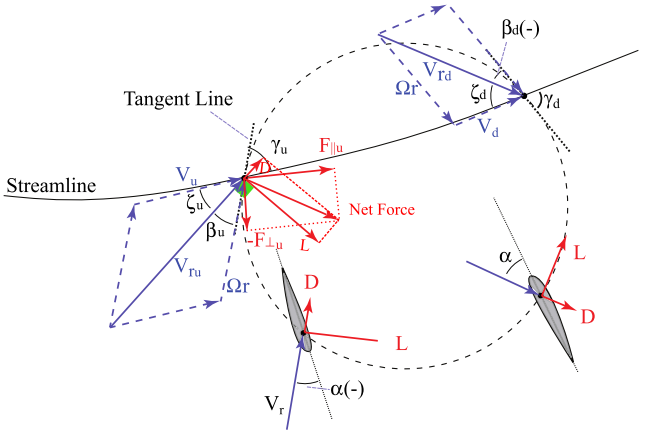

Fig. 9 Angles pertinent to blade element analysis.

dynamic lift and poststall behavior [24,26,28–30]. In the present analysis, the method by Rathi [29] is adjusted to account for curvilinear flow [31] by combining the result from the thin airfoil theory with a polynomial fit of poststall data by Critzos and Heyson [32] to provide the aerodynamic coefficients at full 360 deg angles of attack. To compute the lift and drag coefficients, the Oswald efficiency factor e, the parasite drag coefficient C_{D_o}, the blade aspect ratio, as well as the positive and negative stalling angles of attack must be specified.

Once the lift and drag forces are known, they may be related to the forces on each streamline. A central assumption of flux-line analysis is steady flow. However, the force of each blade on the flow from an Eulerian perspective is unsteady for a finite number of blades, which is considered by time averaging. The blade force is distributed over the chord of the blade c, of which n blades only cover σ portion of the rotor circumference:

$$F = F_{\text{blade}}\frac{\sigma}{c} \tag{47}$$

where solidity for the cycloturbines is as follows:

$$\sigma = \frac{nc}{2\pi r} \tag{48}$$

The distributed lift and drag forces are thus both dependent on the chord length. Because the aerodynamic moment

$$\left(m = \sigma\left(\frac{1}{2}\rho V_r^2 C_m c\right)\right)$$

is due to the production of vorticity, its interaction with the flow cannot be modeled with this quasi-one-dimensional theory. For this reason, it is omitted from the analysis. If desired, it can be integrated into the blade element model to correct its effect on the power. Then, the forces parallel and perpendicular to the streamline for the upstream and downstream flux lines are

$$f_{\|u}(s) = \frac{1}{2}\rho V_{r_u}^2\sigma[C_d(\alpha_u)\cos\zeta_u - C_l(\alpha_u)\sin\zeta_u] \tag{49}$$

$$f_{\perp u}(s) = \frac{1}{2}\rho V_{r_u}^2\sigma[C_l(\alpha_u)\cos\zeta_u + C_d(\alpha_u)\sin\zeta_u] \tag{50}$$

$$f_{\|d}(s) = \frac{1}{2}\rho V_{r_d}^2\sigma[C_d(\alpha_d)\cos\zeta_d + C_l(\alpha_d)\sin\zeta_d] \tag{51}$$

and

$$f_{\perp d}(s) = \frac{1}{2}\rho V_r^2\sigma[C_l(\alpha_d)\cos\zeta_d - C_d(\alpha_d)\sin(\zeta_d] \tag{52}$$

where C_l and C_d are the lift and drag coefficients, respectively.

2. Forces

Similarly, force components (per unit length in the z direction) on the rotor can also be determined by integration over the upstream and downstream flux lines:

$$F_{u_x} = \int_{\phi_u(s=0)}^{\phi_u(s=1)}\Big[f_{\|u}(s)\cos(\phi_u(s)-\gamma_u(s)) - f_{\perp u}(s)\sin(\phi_u(s)-\gamma_u(s))\Big]r\cdot \mathrm{d}\phi_u \tag{53}$$

$$F_{d_x} = \int_{\phi_d(s=0)}^{\phi_d(s=1)}\Big[f_{\|d}(s)\cos(\phi_d(s)-\gamma_u(s)) - f_{\perp d}(s)\sin(\phi_d(s)-\gamma_u(s))\Big]r\cdot \mathrm{d}\phi_d, \tag{54}$$

$$F_{u_y} = \int_{\phi_u(s=0)}^{\phi_u(s=1)}\Big[f_{\|u}(s)\sin(\phi_u(s)-\gamma_u(s)) + f_{\perp u}(s)\cos(\phi_u(s)-\gamma_u(s))\Big]r\cdot \mathrm{d}\phi_u \tag{55}$$

$$F_{d_y} = \int_{\phi_d(s=0)}^{\phi_d(s=1)}\Big[f_{\perp d}(s)\cos(\phi_d(s)-\gamma_d(s)) - f_{\|d}(\phi_d)\sin(\phi_d(s)-\gamma_u(s))\Big]r\cdot \mathrm{d}\phi_d \tag{56}$$

The resultant force applied on the rotor disk is then

$$\boldsymbol{F} = (F_{u_x} + F_{d_x})\hat{i} + (F_{u_y} + F_{d_y})\hat{j} \tag{57}$$

where $\hat{i}$ and $\hat{j}$ are unit directional vectors along the x and y directions, respectively.

3. Aerodynamic Power

The aerodynamic power (per unit length in the z direction) collected by each streamtube is

$$d\boldsymbol{P}_u = -(f_{\|u}\cos\gamma_u + f_{\perp u}\sin\gamma_u)\Omega\cdot r\,\mathrm{d}\phi_u \tag{58}$$

at the upstream flux line and

$$d\boldsymbol{P}_d = (f_{\|u}\sin\gamma_d - f_{\perp d}\sin\gamma_d)\Omega\cdot r\,\mathrm{d}\phi_d \tag{59}$$

at the downstream flux line. The total power is determined by integrating over the rotor disk:

$$\boldsymbol{P} = \int_0^1 \frac{\mathrm{d}\boldsymbol{P}_u}{\mathrm{d}\phi_u}\frac{\mathrm{d}\phi_u}{\mathrm{d}s}\,\mathrm{d}s + \int_0^1 \frac{\mathrm{d}\boldsymbol{P}_d}{\mathrm{d}\phi_d}\frac{\mathrm{d}\phi_d}{\mathrm{d}s}\,\mathrm{d}s \tag{60}$$

The power coefficient is then

$$C_P = \frac{\boldsymbol{P}}{0.5\rho V_\infty^3 A_{\text{projected}}} = \frac{\boldsymbol{P}}{\rho V_\infty^3 r} \tag{61}$$

E. Flux-Line Theory: Summary

Collectively, the preceding elements predict turbine power and forces from specification of the turbine geometry, blade pitching motions (or angle of attack), and the operating conditions (wind speed, rotational speed, air density, etc.). Because the flux-line

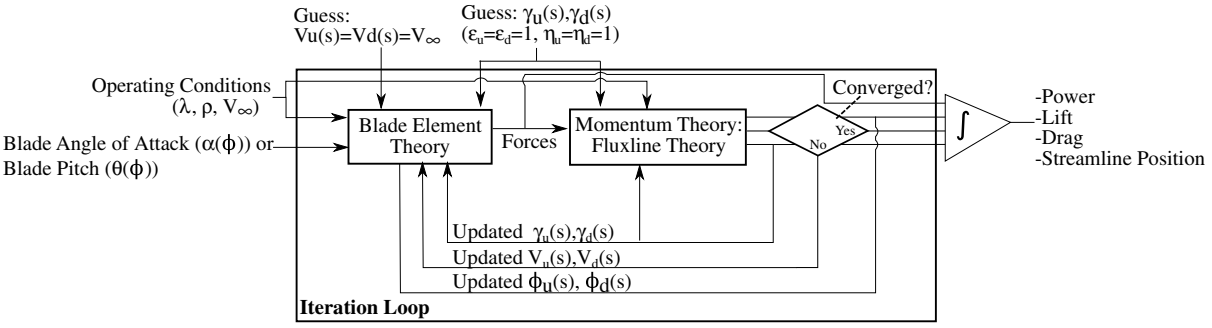

Fig. 10 Block diagram of flux-line execution in a blade element momentum theory.

description of the flow through the turbine requires knowledge of the forces (whereas the blade element model requires specification of the flow conditions), the analysis is implemented in an iterative approach, as shown in Fig. 10. The basic procedures are as follows:

1) The user must preprescribe the fluid properties (density, etc.), blade specifications (airfoil model with lift–drag characteristics, chord length, span length, etc.), turbine geometries (rotor radius, etc.), and operating conditions (wind speed, rotation speed, etc.), as well as an applied blade pitching motion [given $\theta(\phi)$].

2) Initially, the fluid conditions passing the rotor disk are guessed to be those of the freestream flow [i.e., the velocity distributions are the freestream velocity $V_u(s) = V_d(s) = V_\infty$] and the γ distributions approximate that of $\gamma_u(s) = \gamma_d(s) = \arccos(1–2s)$ by choosing $\epsilon_u = \epsilon_d = 1$ and $\eta_u = \eta_d = 1$ in the two-parameter γ model.

3) Determine ζ and α from Eqs. (43–46), as well as V_r from Eqs. (41) and (42).

4) Model the airfoil lift–drag coefficients and compute the force components $f_{\parallel u}$ and $f_{\perp u}$ to each streamline s from Eqs. (49–52).

5) The forces are used in the flux-line momentum model to calculate the fluid velocity $[V_u(s), V_d(s)]$, position $[\phi_u(s), \phi_d(s)]$, and direction $[\gamma_u(s), \gamma_d(s)]$ through the rotor.

a) Determine the updated $V_u(s)$ from Eq. (17) and $V_d(s)$ from Eqs. (12) and (21).

b) Determine the freestream area ratio from Eq. (35) and $\phi(s)$ from Eqs. (38) and (39).

6) With the aforementioned updated values, determine the updated coefficients ϵ and η in the two-parameter model by solving integral equations (25) and (28–30). This gives updated expressions of $\gamma_u(s)$ and $\gamma_d(s)$. This system of integral equations must be solved with a root-finding technique or numerical optimization. The present study implements the constrained sequential nonlinear optimization algorithm in the MATLAB function "fmincon."

7) Repeat procedures 3 to 6 until convergence is achieved. Currently, convergence is achieved when the sum of the differences between the induced velocities between adjacent iterations is smaller than a chosen threshold.

8) The converged results are fed into Eqs. (53–56) to compute the force $\boldsymbol{F}$ applied on the rotor disk.

9) The aerodynamic power $\boldsymbol{P}$ is computed from Eqs. (60).

Similar to the aforementioned streamtube models, this newly proposed flux-line theory features a minimal computation cost, but with an improved accuracy by accounting more realistic flow physics (bending and expansion). It can be easily implemented by a desktop computer, with computation lasting from a few minutes to tens of minutes. Thus, once validated, it represents a promising design tool for quickly predicting the performances of different design modifications.

III. Model Validation

For model validation, we compared the predictions of flux-line theory with three sets of published experimental data from cyclorotor tests, for which the details are summarized in Table 1. Vandenberghe and Dick measured power, rotational speed, and wind velocity on a cyclorotor [14,33] by using a cam-based pitch adjustment mechanism predicted to be optimal based on previous theoretical and wind-tunnel investigations. Madsen and Lundgren [34] reported a similar experiment by applying a pitch scheme of $\theta(\phi) = 6.6 \sin\phi + 3.1$ (in degrees). Benedict et al. performed a small-scale wind-tunnel experiment by varying the phase and amplitude of a near-sinusoidal pitching motion [1].

Figure 11 compares the various model predictions with measurements by Vandenberghe and Dick [33]. All models predict the power coefficient well at low loading conditions (in this case, also low TSRs), where there is little flow bending and the momentum exchange is small. As the TSR increases, there is more momentum exchange and disparities emerge. The flux-line theory predicts the trend of the power reduction at $\lambda > 2.5$, but it slightly underpredicts the magnitude of C_p. The single streamtube model fails to predict the trend at a higher TSR, and other models severely underpredict C_p.

The predictions from the flux-line theory also agree well with experiments by Madsen and Lundgren [34], as shown in Fig. 12. These experiments collected data over a longer period of time and experienced different turbulent conditions, which led to the scattered appearance of experimental data in Fig. 12 despite the implementation of averaging [34]. The flux-line theory provides the best estimate of the highest density of experimental data points.

Table 1 Experimental conditions

Category	Vandenberghe and Dick [14,33]	Madsen and Lundgren [34]	Benedict et al. [1]
Radius r, m	1.825	1.4	0.127
Span b, m	2.4	3.3	0.254
Chord c, m	0.365	0.28	0.034
Solidity σ	0.0955	0.095	0.169
Chord-to-radius ratio c/r	0.152	0.084	0.114
Rotor aspect ratio $b/2r$	0.66	1.18	1
Blade airfoil	NACA0012	NACA0015	NACA0015
Number of blades n	3	3	4
Pitching axis location, % c	25%	Not available	25%
Pitching scheme	Second-order optimum	Sinusoidal	Near sinusoidal
Freestream velocity V_∞, m/s	Variable	Variable	10
Tip speed ratio λ range	1.5–3	1–3.7	0.2–1.1
$Re = (cV_\infty\sqrt{1+\lambda^2}/\nu)$	300,000–800,000	150,000–450,000	23,000–35,000
Experimental conditions	Open air	Open air	Open-jet wind tunnel

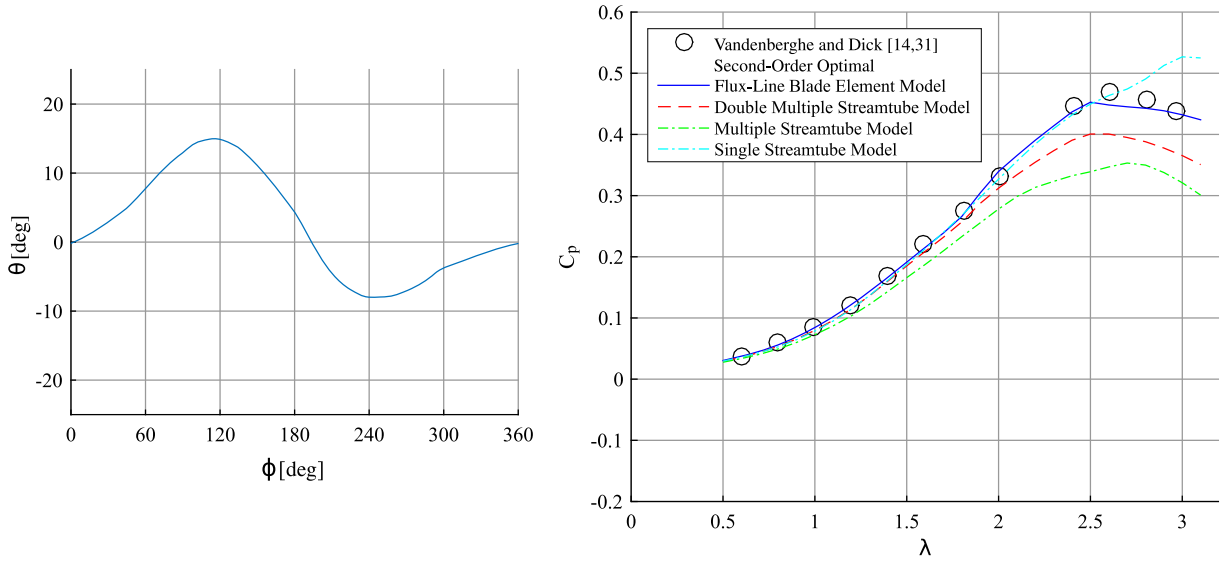

Fig. 11 Blade pitch adjustment scheme adopted by Vandenberghe and Dick experimental cycloturbine (left) [14,33]; and comparison of predictions from flux-line theory, DMS, MS, and SS models with measurement data (right). The experimental result represents the net power from the blades, which excludes the parasite power loss from the rotor structure. An identical steady blade element model from Rathi [29] was implemented with an adjustment for curvilinear flow via Miglore et al. [31] for all momentum models. The following parameters were selected in the model analysis: interior stalling angle of attack of 25 deg, exterior stalling angle of attack of 15 deg, parasite drag coefficient of 0.022, and Oswald efficiency factor of 0.85. Flow through the turbine was discretized into 30 streamtubes.

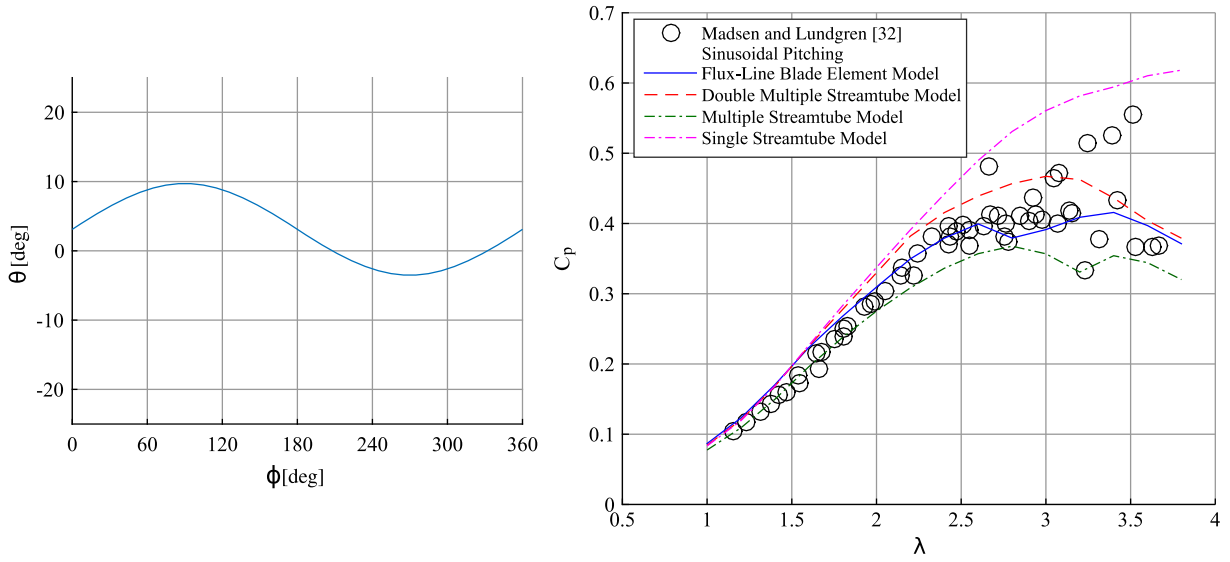

Fig. 12 Madsen and Lundgren [34] experimental cycloturbine blade pitch adjustment scheme (left); and comparison of flux-line theory, DMS, MS, DSS, and SS models with data (right). The experimental data are mathematically adjusted for net power from the gross aerodynamic power by Madsen et al. An identical steady blade element model from Rathi [29] was implemented, with adjustment for curvilinear flow via Migliore et al. [31] for all momentum models. The following parameters were selected: interior stalling angle of attack of 25 deg, exterior stalling angle of attack of 15 deg, parasite drag coefficient of 0.018, and Oswald efficiency factor of 0.85. Flow through the turbine was discretized into 30 streamtubes.

Presumably, this suggests that it most accurately predicts the true turbine efficiency in a controlled test with consistent atmospheric turbulence. At low TSRs, all of the theories give matched results, but they slightly overpredict the experimental data. Likely, this is a result of an improperly matched blade element model, because there is nearly uniform flow at low turbine loading conditions.

The flux-line theory also accurately models the performance under lower-Reynolds-number and low TSR conditions, which are identical to the ones reported by Benedict et al. [1]. Figure 13 compares the predictions with 10 and 20 deg near-sinusoidal pitching motions on a small cycloturbine. The flux-line theory slightly overpredicts the power at all TSRs in both tests but provides a better estimate than the other streamtube theories. Again, the discrepancy between prediction and measurement is amplified with the increased TSR and turbine loading. This accurate modeling is accomplished in a negligible computational time on an ordinary desktop computer. Consequently, the model is tractable for implementation in optimization algorithms, where many iterations are required.

As a low-order model, the flux-line theory has unavoidable limitations. First, it computes the wake velocity by assuming a total pressure loss across the flux line and then a full expansion of the wake flow to ambient pressure. This assumption is valid in the far wake of the turbine but is questionable within the rotor disk. Therefore, it likely overestimates the flow expansion and underpredicts the downstream induced velocity. In the case of a highly loaded rotor front and lightly loaded rear, the model will underpredict the power coefficient. In no case will the enforcement of flow expansion cause an overprediction of the power coefficient. Second, a numerical iteration is required to combine the blade element portion of the model with the momentum method for rapid results. To do so, the flux

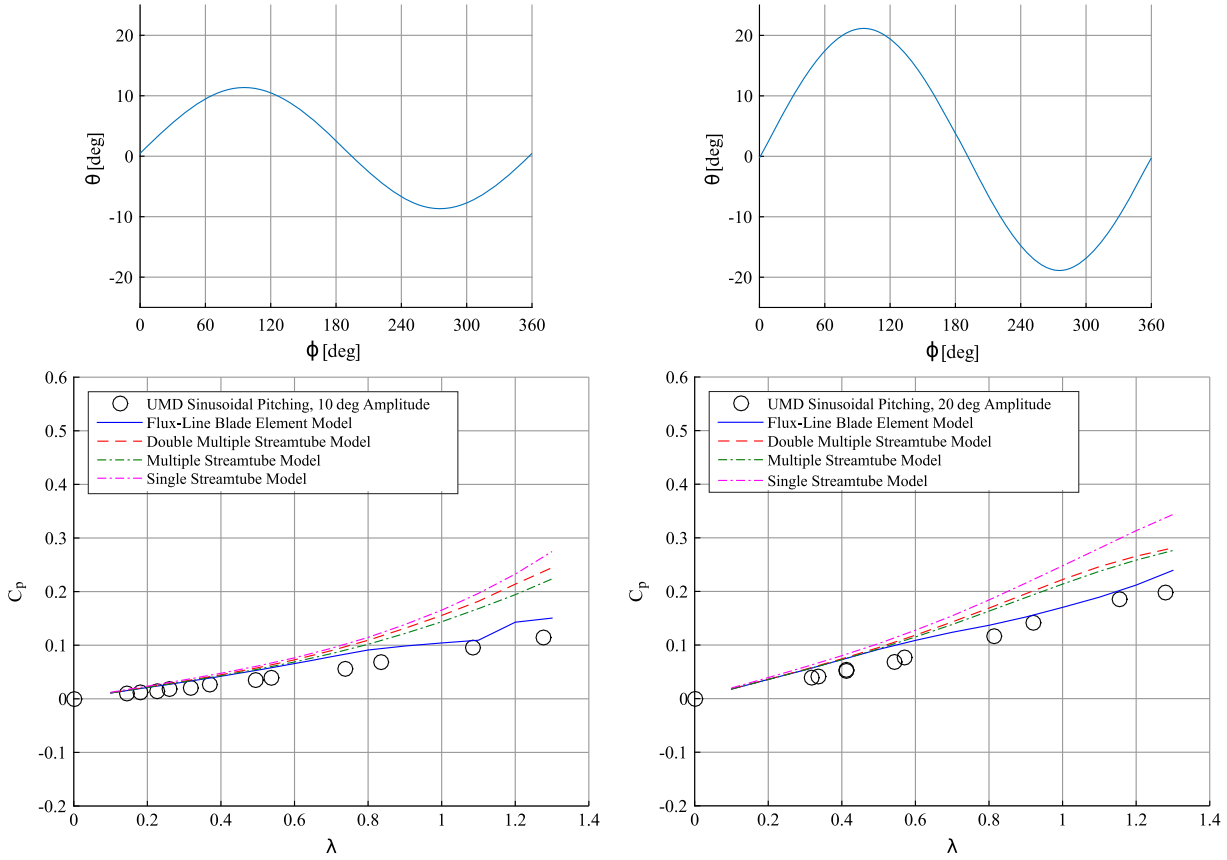

Fig. 13 Blade pitch motion adopted in experimental cycloturbine by Benedict et al. at the University of Maryland (UMD) for pitch amplitudes of 10 deg (left) and 20 deg (right), respectively (top) [1]. Comparison of predictions from flux-line theory, DMS, MS, DSS, and SS models with measurements (bottom). The symbols represent the measured net power from the blades, which excludes the parasite power loss from the rotor structure. An identical steady blade element model from Rathi [29] was implemented, with adjustment for curvilinear flow via [31] for all momentum models. The following parameters were selected: interior stalling angle of attack of 28 deg, exterior stalling angle of attack of 9 deg, parasite drag coefficient of 0.02, and Oswald efficiency factor of 0.85. Flow through the turbine was discretized into 30 streamtubes.

lines must be discretized by the streamline index s. However, this creates nonsensible solutions at many turbine operating conditions because the portion of the rotor circumference encompassed by the two near endpoints is greatly exaggerated. Near $s = 0$ and $s = 1$, the values of γ_u and γ_d approach zero. Consequently, the contribution of term

$$\frac{V_\infty}{V_u(s)\sin(\gamma_u(s))}$$

becomes significant in the expressions for $\mathrm{d}y_\infty/\mathrm{d}s$, $\mathrm{d}\phi_u/\mathrm{d}s$, and $\mathrm{d}\phi_d/\mathrm{d}s$. In principle, this is not a problem because the portion of the s domain that they encompass is small. However, when the model is discretized, these large values are disproportionately represented. In turn, the functions $\phi_u(s)$ and $\phi_d(s)$ may be erroneously predicted. This shortcoming can be mitigated by varying the spacing of the discretization points, limiting the range of γ_u and γ_d to a value somewhat above zero and below π, or capping the value described of

$$\frac{V_\infty}{V_u(s)\sin(\gamma_u(s))}$$

The second method is most easily implemented and chosen in the current study.

IV. Flux-Line Pure Momentum Theory

The preceding blade element momentum implementation of the flux-line theory provides an effective cycloturbine design and evaluation tool. Moreover, when the dependence on the blade element model is eliminated, the flux-line theory provides general insights into cycloturbine flow physics. A key conclusion of this analysis is the establishment of a performance limit akin to the Betz limit prescribed for HAWTs. In this "pure" momentum implementation of the flux-line theory, interference factors are prescribed for the upstream and downstream flux lines that are similar to the induction factor in the one-dimensional (1-D) actuator disk model for HAWTs instead of detailed blade geometry and pitching motions. The interference factors a_u and a_d for the upstream and downstream flux lines are introduced by

$$a_u V_\infty = V_\infty - V_u \tag{62}$$

and

$$a_d V_{u_{\text{wake}}} = V_{u_{\text{wake}}} - V_d \tag{63}$$

Following a similar analysis as in the 1-D actuator disk model, one has

$$2a_u V_\infty = V_\infty - V_{u_{\text{wake}}} \tag{64}$$

and

$$2a_d V_{u_{\text{wake}}} = V_{u_{\text{wake}}} - V_w \tag{65}$$

Rearranging yields

$$V_u = V_\infty(1 - a_u) \tag{66}$$

$$V_{u_{\text{wake}}} = V_\infty(1–2a_u) \tag{67}$$

$$V_d = V_{u_{\text{wake}}}(1 - a_d) = V_\infty(1–2a_u)(1 - a_d) \tag{68}$$

$$V_w = V_{u_{\text{wake}}}(1–2a_d) = V_\infty(1–2a_u)(1–2a_d) \tag{69}$$

These equations can be combined with the results of the momentum theory analysis. Starting with the upstream flux line, multiplying Eq. (14) by V_u yields

$$V_{u_{\text{wake}}} V_u = V_\infty V_u - \frac{f_{\parallel u}}{\rho \sin\gamma_u} \tag{70}$$

Substituting in Eqs. (66) and (67) gives

$$V_\infty^2(1 - a_u)(1–2a_u) = V_\infty^2(1 - a_u) - \frac{f_{\parallel u}}{\rho \sin\gamma_u} \tag{71}$$

which simplifies to

$$a_u(1 - a_u) = \frac{f_{\parallel u}}{2\rho V_\infty^2 \sin\gamma_u} \tag{72}$$

or, alternatively,

$$f_{\parallel u} = 2\rho V_\infty^2 a_u(1 - a_u)\sin\gamma_u \tag{73}$$

The same analysis can be performed on the downstream flux line, yielding [starting from Eq. (19)]

$$f_{\parallel d} = 2\rho \sin\gamma_d V_\infty^2(1–2a_u)^2(1 - a_d)a_d \tag{74}$$

For a turbine blade operated under normal conditions, the lift force is significantly greater than the drag force, which is thus neglected in the following analysis to estimate the optimal power. This simplification allows the force parallel to each streamline (as shown in Fig. 9 when $D = 0$) to be related to the force perpendicular to each streamline:

$$\frac{f_{\parallel u}}{-\sin\zeta_u} = \frac{f_{\perp u}}{\cos\zeta_u} \tag{75}$$

Similarly,

$$\frac{f_{\parallel d}}{\sin\zeta_d} = \frac{f_{\perp d}}{\cos\zeta_d} \tag{76}$$

Rearranging gives the perpendicular streamline forces as functions of the interference factors

$$f_{\perp u} = \frac{-f_{\parallel u}}{\tan\zeta_u} = \frac{-2\rho V_\infty^2 \sin\gamma_u a_u(1 - a_u)}{\tan\zeta_u} \tag{77}$$

and

$$f_{\perp d} = \frac{f_{\parallel d}}{\tan\zeta_d} = \frac{2\rho V_\infty^2 \sin\gamma_d(1–2a_u)^2 a_d(1 - a_d)}{\tan\zeta_d} \tag{78}$$

Note that

$$\tan\zeta_u = \frac{\Omega r \sin\gamma_u}{\Omega r \cos\gamma_u + V_u} = \frac{\lambda \sin\gamma_u}{\lambda \cos\gamma_u + (1 - a_u)} \tag{79}$$

Now, the power can be written exclusively in terms of the tip speed ratio, turbine geometry, and the upstream and downstream interference factors. Note that these interference factors are functions of the flux-line coordinate s, i.e., $a_u(s)$ and $a_d(s)$. The differential power is

$$dP_u = V_u f_{\parallel u} r d\phi_u = 2\rho V_\infty^3 \sin\gamma_u a_u(1 - a_u)^2 r d\phi_u \tag{80}$$

and

$$dP_d = V_d f_{\parallel d} r d\phi_d = 2\rho V_\infty^3 \sin\gamma_d(1–2a_u)^3 a_d(1 - a_d)^2 r d\phi_d \tag{81}$$

Rewriting the transformation equations produces a term for the flux-line spatial derivatives in terms of the interference factors:

$$\frac{\mathrm{d}y_\infty}{\mathrm{d}s} = \frac{2r\pi}{\int_0^1 (ds/(1 - a_u)\sin(\gamma_u(s))) + \int_0^1 (ds/(1–2a_u)(1 - a_d)\sin(\gamma_d(s)))} \tag{82}$$

From Eq. (60), the power is

$$P = \int_0^1 \frac{\mathrm{d}P_u}{\mathrm{d}\phi_u}\frac{\mathrm{d}\phi_u}{\mathrm{d}s}\,\mathrm{d}s + \int_0^1 \frac{\mathrm{d}P_d}{\mathrm{d}\phi_d}\frac{\mathrm{d}\phi_d}{\mathrm{d}s}\,\mathrm{d}s \tag{83}$$

which is expanded to

$$P = 2\rho V_\infty^3 \frac{\mathrm{d}y_\infty}{\mathrm{d}s}\left(\int_0^1 a_u(1 - a_u)\,\mathrm{d}s + \int_0^1 (1–2a_u)^2 a_d(1 - a_d)\,\mathrm{d}s\right) \tag{84}$$

The coefficient of power is calculated directly from the total power:

$$C_p = 4\pi \frac{\int_0^1 a_u(s)(1 - a_u(s))\,\mathrm{d}s + \int_0^1 (1–2a_u(s))^2 a_d(s)(1 - a_d(s))\,\mathrm{d}s}{\int_0^1 (ds/(1 - a_u(s))\sin(\gamma_u(s))) + \int_0^1 (ds/(1–2a_u(s))(1 - a_d(s))\sin(\gamma_d(s)))} \tag{85}$$

Because the velocity through the rotor is initially specified, iteration is not required. The angles $\gamma_u(s)$ and $\gamma_d(s)$ must be modeled. The two-parameter model previously described is used. Consequently, the flux-line pure momentum theory predicts the performance of a cycloturbine based only on the specification of the interference functions.

A. Establishment of a Theoretical Performance Limit

The flux-line pure momentum theory places a theoretical performance limit for VAWTs similar to the Betz limit for HAWTs. This limit is obtained by optimizing the distributions of $a_u(s)$ and $a_d(s)$ to maximize the coefficient of power in Eq. (85). The distributions $\gamma_u(s)$ and $\gamma_d(s)$ must be modeled and have a strong effect on the maximum power coefficient. The following section provides a numerical optimization routine employing the two-parameter model described previously. Alternatively, the interference distributions can be fixed as constants in a simplified analytical analysis.

1. Numerical Optimization for Determination of Performance Limit

For numerical optimization, the efficient internal point nonlinear sequential constrained optimization technique is implemented via the MATLAB function fmincon, which requires a finite number of design variables rather than optimization functions. Consequently, the distributions of interference factors $a_u(s)$ and $a_d(s)$ are approximated by a series of design variables x_i, $i = 1{:}\ l$, with an applied cubic polynomial interpolation along each function. A convergence study determines that 11 points ($l = 11$) are required to adequately define the interference functions for a coefficient of power within 0.01.

The generated functions are evaluated by constraint functions. Also, $a_u(s)$ and $a_d(s)$ are constrained by the maximum lift that the blades can generate:

$$L \leq \frac{1}{2}\rho V_r^2 \sigma C_{L_{\max}} \tag{86}$$

A range of rotor solidities and a maximum blade lift coefficient of 2.5 are selected. To enforce the determination of smooth and reasonable functions, the derivative

$$\left(\frac{\mathrm{d}a_u}{\mathrm{d}s}, \frac{\mathrm{d}a_d}{\mathrm{d}s}\right)$$

and the second derivative of the interference functions

$$\left(\frac{\mathrm{d}^2a_u}{\mathrm{d}s^2}, \frac{\mathrm{d}^2a_d}{\mathrm{d}s^2}\right)$$

are constrained to reasonable ranges:

$$\left|\frac{\mathrm{d}a}{\mathrm{d}s}\right| < 4\frac{1}{\mathrm{rad}}$$

and

$$\left|\frac{\mathrm{d}^2a}{\mathrm{d}s^2}\right| < 1\frac{1}{\mathrm{rad}^2}$$

Furthermore, to ensure a positive far-wake velocity, the following constraint function is applied:

$$(1\text{–}2a_u)^2(1\text{–}2a_d) > 0 \tag{87}$$

If the power is maximized under only these constraints, the solution is unbounded and there is no limit to the maximum turbine power. In those unbounded solutions, the upstream flux-line interference function is less than zero and the downstream distribution greater than zero. This corresponds to a dual propeller-turbine operating mode. Theoretically, the upstream portion of the turbine puts power into the flow, which accelerates and contracts a larger freestream area of wind than the actual projected turbine area ($a_u < 0$, $(A_\infty/A_{\text{projected}}) > 1$). Then, the downstream portion of the turbine retards ($a_d > 0$) and isentropically extracts the greater total wind energy. In this model, the freestream area ratio is greater than one, and the wake velocity is less than the freestream velocity, as shown in Fig. 14. Mounting higher-order system inefficiencies may make this combined propeller-turbine operating mode difficult or impossible to realize. However, the idea warrants future in-depth evaluation.

To place a more realistic limit on system power, the interference functions were further constrained to only positive values less than 0.5, i.e., $0 \leq a_u(s) \leq 0.5$ and $0 \leq a_d(s) \leq 0.5$. This forces turbine-only operation, where all portions of the turbine are only permitted to decelerate the flow. The sequential constrained optimization routine identified the most efficient interference distributions at a range of tip speed ratios, as depicted in Fig. 15. The performance limit for a VAWT is found by computing C_p for these interference distributions over a range of tip speed ratios. This dependence is compared with other performance limits in Fig. 16. The flux-line theory suggests that, to yield the optimum power, the upstream flux line should not decelerate the flow (working at a zero loading status) and the downstream flux line should decelerate the flow to just under 2/3 (i.e., $a_d \gtrsim 1/3$) of the freestream value at moderate TSRs. Blade pitch motions should then be designed to produce the interference factors in Fig. 15 for optimum performance. The mechanism for this power extraction is a greater effective area over the downstream portion of the turbine, which is explained in Sec. IV.A.3.

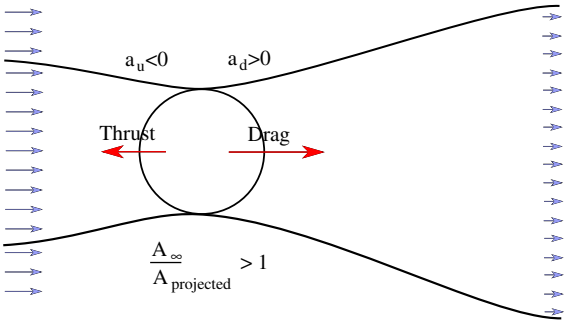

Fig. 14 Isentropic cycloturbine with infinite blades that could contract an area of freestream flow greater than the projected area of the rotor through utilization of cyclorotor pitching kinematics in the front half of the turbine. The flow could then be expanded in the rear half for a coefficient of power greater than one.

These interference distributions produce a maximum cycloturbine coefficient of power that increases from zero to a limit of 0.597 with increasing TSR. This represents only a marginal improvement from the 1-D Betz limit of 0.593 [35]. The rate of performance increase steepens with solidity because those rotors can exert greater deceleration forces on the fluid for the same available blade relative velocity. In theory, the cycloturbine maximum power coefficient exceeds the rotating HAWT limit [27] at TSRs near two to three. Historically, cycloturbines have been designed with low solidity for operation at high TSRs. However, they were often constrained to TSRs less than three to limit rotational speed for structural reasons or achieved low performance at high TSRs due to support structure drag losses. The performance of turbines can be improved by using a larger rotor solidity and maintaining only moderate TSRs. However, increasing the solidity will also magnify blade parasite drag from the additional area and induced drag from reduced blade aspect ratio. Consequently, there will be a design solidity and rotational speed that provides the best power that will depend on the exact aerodynamic characteristics of the geometry. This tradeoff deserves additional consideration in a future study.

It must be cautioned that this flux-line performance limit is sensitive to the model selected for $\gamma_u(s)$ and $\gamma_d(s)$. Other models will provide different values. The dependence of the maximum coefficient of power and the optimum interference distributions on the inflow model is explored next.

2. Simplified Analytical Analysis of Maximum Performance

An alternative optimization technique is to select interference functions for $a_u(s)$ and $a_d(s)$ that are dependent only on a variable interference constant. The simplest choice is to suppose that these distributions are constants, i.e., $a_u(s) = A_u$ and $a_d(s) = A_d$. Substituting into Eq. (85) yields

$$C_p = 4\pi \frac{A_u(1-A_u) + (1\text{–}2A_u)^2 A_d(1-A_d)}{(1/1-A_u)\int_0^1 (ds/\sin\gamma_u) + (1/(1\text{–}2A_u)(1-A_d))\int_0^1 (ds/\sin\gamma_d)} \tag{88}$$

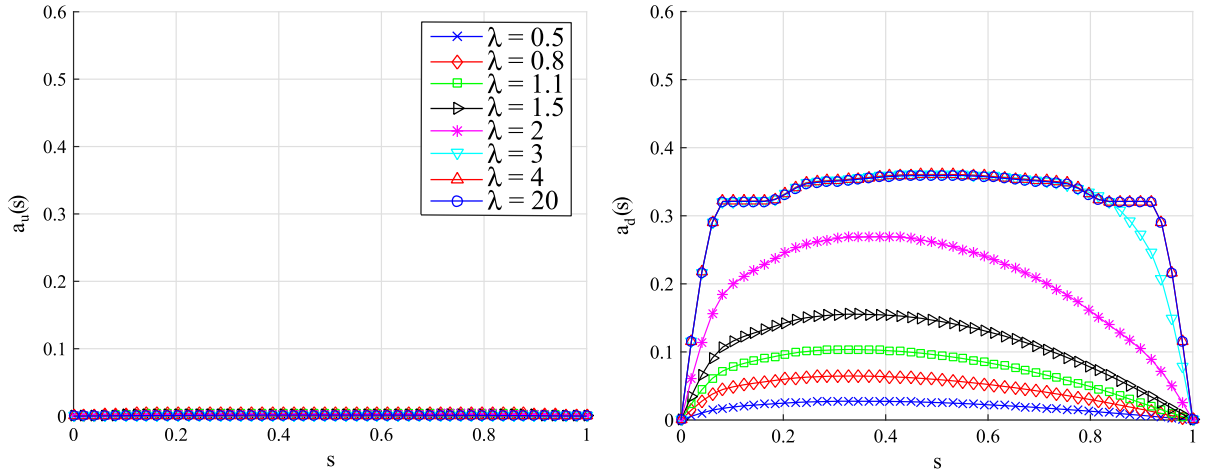

Fig. 15 Optimum distributions of interference factors: $a_u(s)$ (left) and $a_d(s)$ (right) for a rotor solidity of 0.2.

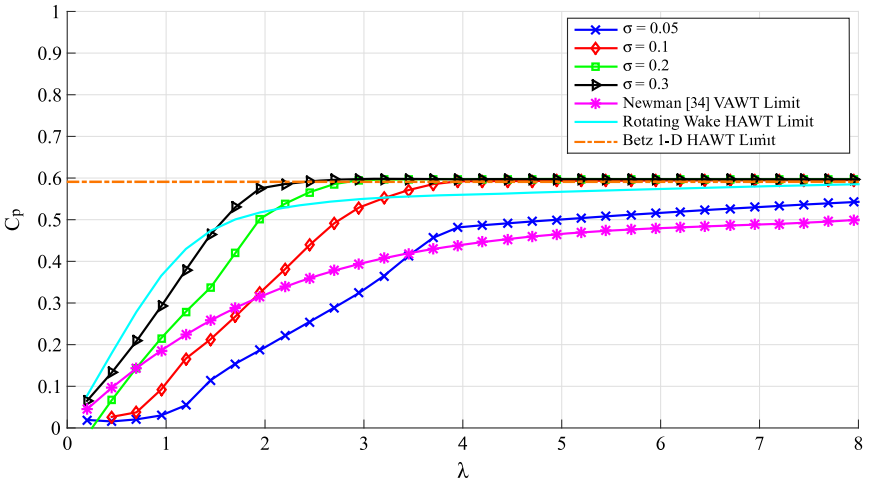

Fig. 16 Comparison of the flux-line theory performance limit with other wind turbine performance limits for varying rotor solidity. The rotating wake HAWT limit and Betz 1-D limit are not applicable to VAWTs and are presented for comparison only.

If the ratio of integrals is defined as a variable κ

$$\kappa = \frac{\int_0^1 (ds/\sin\gamma_d)}{\int_0^1 (ds/\sin\gamma_u)} \tag{89}$$

then the coefficient of power function simplifies to

$$C_p = \frac{4\pi}{\int_0^1 (ds/\sin\gamma_u)} \frac{A_u(1-A_u) + (1\text{–}2A_u)^2 A_d(1-A_d)}{(1/(1-A_u)) + (\kappa/(1\text{–}2A_u)(1-A_d))} \tag{90}$$

This expression is convenient to evaluate: if

$$\int_0^1 \frac{ds}{\sin\gamma_u}$$

is taken as a constant for small variations in the interference distribution constants, the partial derivatives depend only on the ratio of the γ distribution integrals but not their explicit value. Figure 17 plots Eq. (90) for

$$\int_0^1 \frac{ds}{\sin\gamma_u} = \frac{\pi}{2}$$

and $\kappa = 1$. In these plots, there is no clear local maximum due to the presence of combined propeller-turbine operating modes (denoted in the right contour plot) that theoretically have an unbounded coefficient of power. Again, the feasibility of this operating regime requires further investigation.

Determining the root of the partial derivative $(\partial C_p/\partial A_d) = 0$ at $A_u = 0$ provides the optimum interference coefficient values for the turbine-only operating mode. These values are plotted in Fig. 18. The interference constants are nearly constant over a wide range of κ ($A_u = 0$ and $0.38 < A_d < 0.39$). Thus, the optimum interference constants are quasi independent of the actual γ distributions. This eliminates the requirement to model those distributions to obtain an efficient distribution. However, the maximum C_p still requires computation of both γ distributions. The potential values of this are plotted on the right side of Fig. 18. For the expansion of flow in a turbine, $\kappa < 1$. For the unloaded turbine, we have $\gamma = \arccos(1\text{–}2s)$; thus,

$$\int_0^1 \frac{ds}{\sin\gamma_u} = \frac{\pi}{2}$$

and for a loaded cycloturbine, we have

$$\int_0^1 \frac{ds}{\sin\gamma_u} > \frac{\pi}{2}$$

Consequently, this narrows the maximum C_p region to that shown on the right of Fig. 18. Because the flow expansion should not be dramatic,

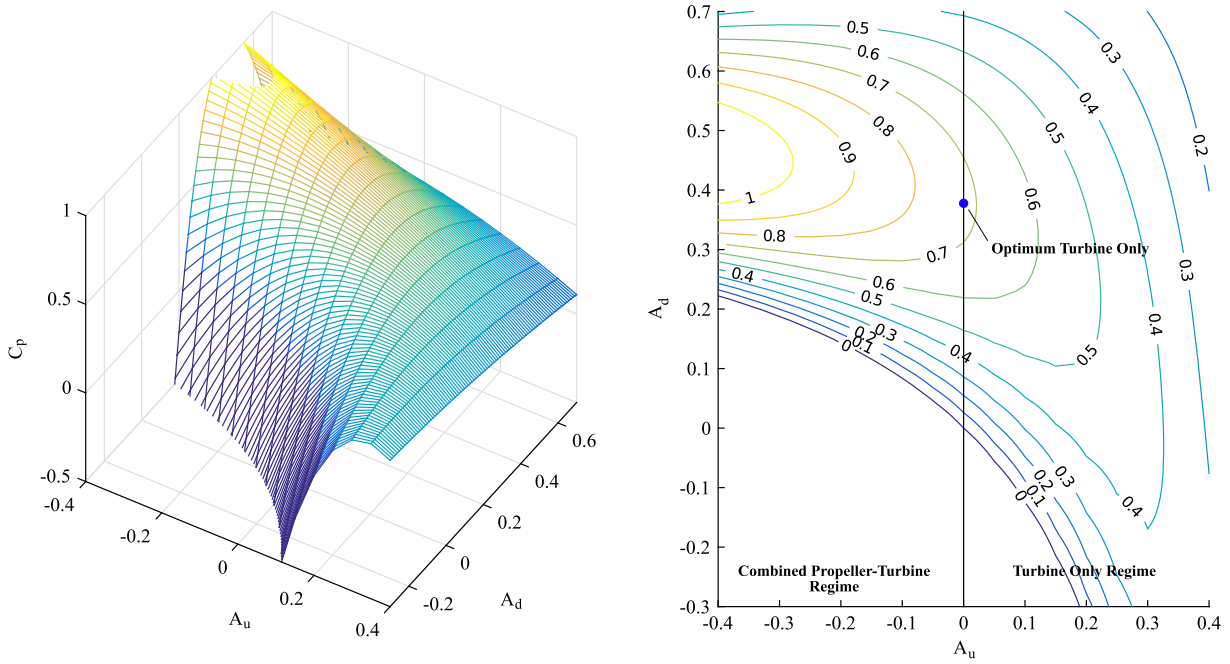

Fig. 17 Variation of coefficient of power for a constant interference distribution over the upstream and downstream flux lines with $\int_0^1 (ds/\sin\gamma_u) = (\pi/2)$ and $\kappa = 1$. The mesh surface (left) and contour plot (right) are equivalently colored at constant C_p values.

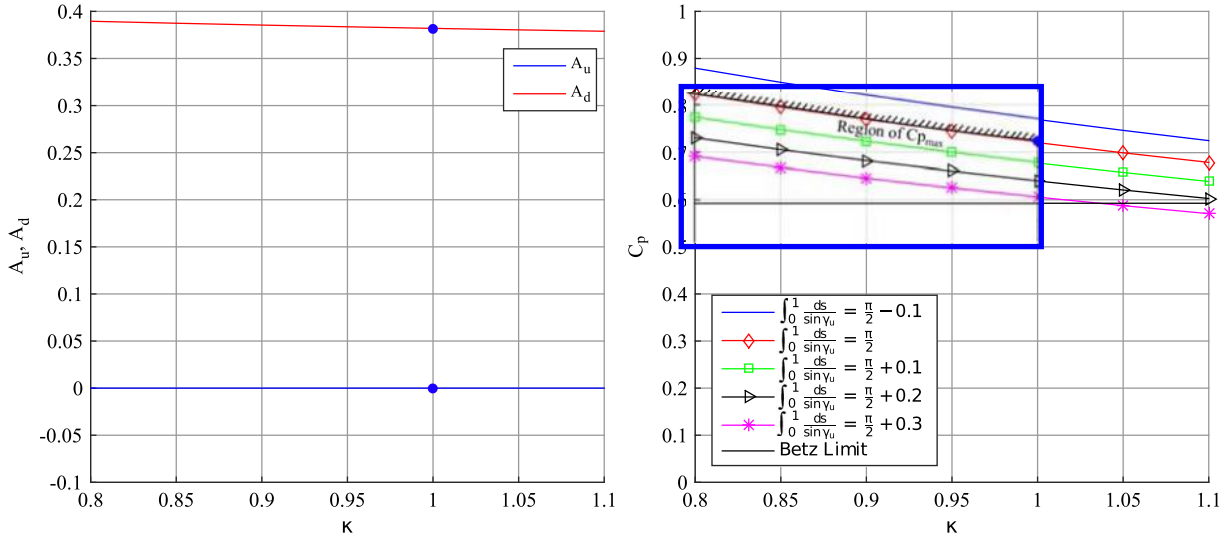

Fig. 18 Variation of interference factor constants for varying distributions of γ_u and γ_d (left) and the corresponding maximum power coefficient (right). For flow expanding in a turbine mode, $\kappa < 1$ and $\int_0^1 (ds/\sin\gamma_u) > (\pi/2)$. These conditions bound the region of potential $C_{p_{max}}$, as shown in the right panel.

$$\int_0^1 \frac{ds}{\sin\gamma_u}$$

should not substantially exceed $\pi/2$; thus, the maximum theoretical power that can be extracted by a cycloturbine should slightly exceed the Betz limit. However, a better understanding of the actual γ distributions is necessary to provide a precise limit.

The blue point in Figs. 17 and 18 provides an example for mathematical consideration. At these point, $A_u = 0$,

$$\int_0^1 \frac{ds}{\sin\gamma_u} = \frac{\pi}{2}$$

and $\kappa = 1$; so,

$$C_p = \frac{4\pi}{\int_0^1 (ds/\sin\gamma_u)} \frac{A_d(1-A_d)}{1+(\kappa/(1-A_d))} = \frac{8A_d(1-A_d)^2}{2-A_d} \qquad (91)$$

Solving

$$\frac{\partial C_p}{\partial A_d} = 0$$

suggests that the potential maxima of C_p occurs at $A_d = 1$ and $A_d = (1/2)(3 \pm \sqrt{5})$. Only $A_d = (1/2)(3 - \sqrt{5})$ is physically attainable. Substituting this value into Eq. (91) yields $C_{p_{max}} = 0.721$.

3. *Mechanism for Higher-Than-Betz Power Extraction*

Cycloturbines achieve a higher coefficient of power by using a larger effective turbine area on the concave surface of the backside of the rotor disk. This larger effective area can access a larger freestream area of wind (the value of dy_∞/ds is closer to two), which causes a higher power coefficient when normalized by the turbine projected area. The effective areas spanned by the upstream and downstream flux lines are given by

$$A_{e_u} = \int_0^1 \sin(\gamma_u)\frac{\mathrm{d}\phi_u}{\mathrm{d}s} r\,\mathrm{d}s = \int_0^1 \frac{1}{(1-a_u)}\frac{\mathrm{d}y_\infty}{\mathrm{d}s}\,\mathrm{d}s \quad (92)$$

and

$$A_{e_d} = \int_0^1 \sin(\gamma_d)\frac{\mathrm{d}\phi_d}{\mathrm{d}s} r\,\mathrm{d}s = \int_0^1 \frac{1}{(1-2a_u)(1-a_d)}\frac{\mathrm{d}y_\infty}{\mathrm{d}s}\,\mathrm{d}s \quad (93)$$

For any turbine-only interference, distribution on the downstream flux line will always have a greater effective area than the upstream flux line. Because flow is expanding through the downstream flux line, the downstream effective area is also greater than the equivalent projected area of the turbine, i.e.,

$$A_{e_d} \geq A_{\text{projected}} \geq A_{e_u} \quad (94)$$

This mechanism is markedly different than that suggested by Newman [36], who used a modified streamtube method to derive a similar performance limit for VAWTs. That mathematical derivation resembled a 1-D double actuator disk theory, where slightly higher theoretical performance ($C_{p_{\max}} = 16/25$) was achieved by incrementally expanding the flow across two actuator disks. Figure 16 presents Newman's theoretical limit, which suggests that VAWTs only marginally exceed the Betz limit at extremely high TSRs [36]. Because streamtube models do not model flow expansion, the effective areas of the upstream and downstream portions of the rotor are equal. In flux-line theory, increasing the interference factor on the upstream portion of the rotor a_u disproportionately reduces the area of the freestream wind processed by the rotor as compared to the downstream interference factor a_d, as shown in Eq. (82). This reduces the advantage of using both the upstream and downstream portions of the rotor for flow deceleration.

V. Conclusions

A novel low-order blade element momentum model for predicting the performance of cycloturbines, named flux-line theory, is developed. It accounts for the bending and expansion/contraction of the flow by computing fluid characteristics along each streamline without a predescribed spatial location. A transformation determines the Cartesian location of streamlines, and additional calculations determine the power and forces produced. Predictions of flux-line theory are validated against three sets of experimental data measured at a range of Reynolds numbers and pitch motions. The new model is extended to flux-line pure momentum theory, which eliminates dependence on the blade element model, to gain insight into optimum blade–fluid interaction. An analysis with this theory identifies the maximum theoretical turbine performance and optimum flow conditions, which is an essential precursor for determining optimal blade pitch kinematics. The following conclusions are drawn from this study:

1) The flux-line theory accurately models the coefficient of power for cycloturbines at a range of TSRs ($0 \leq \lambda \leq 3$) and Reynolds numbers by modeling the flow expansion and bending effects. It predicts the performance more accurately than single, double, single multiple, and double multiple streamtube models implementing the same simple blade element model. The flux-line theory is a useful tool for designing preliminary pitching motions and cycloturbine geometry.

2) The flux-line pure momentum theory eliminates the dependence on a blade element model by adopting distributions of interference factors on the upstream and downstream flux lines (where flow crosses the rotor blade path). This simplified variation of flux-line theory is useful for understanding the aerodynamic characteristics of the cycloturbine system. It suggests that cycloturbines can produce the most power when they are operated in a dual propeller-turbine mode. In this mode, the upstream portion of the turbine acts as a propeller (with energy consumption) and contracts a larger area of the freestream wind; the downstream portion harvests wind energy where the wind is expanded. Flux-line theory provides no theoretical limit to the maximum turbine power production under these circumstances. However, feasible implementation of this concept, where unsteady blade interaction and blade drag will be significant, seems unlikely and requires further investigation.

3) If the cycloturbine is operated in a turbine-only mode, the flux-line pure momentum theory can provide a theoretical vertical-axis wind turbines performance limit through optimization of interference factor distributions $a_u(s)$ and $a_d(s)$. The limit is dependent on the choice of the model used to describe the angle at which the flow crosses the upstream and downstream flux lines. Using a two-parameter model that matches experimental data, the limit is numerically determined as 0.597. A simplified analytical approach determines a range of maximum value of the coefficient of power that is likely greater than $16/27$ but less than 0.8.

4) To harvest the maximum power, the theory suggests that the upstream blades should extract no energy from the flow (operate at zero blade lift coefficient), whereas the downstream blades reduce the velocity by slightly more than one-third of the freestream value. This best power interference function is quasi independent of the choices of the flow angle (γ_u and γ_d) distribution model.

5) Flux-line pure momentum theory suggests that cycloturbines have a higher theoretical power coefficient than horizontal-axis wind turbines because they have a larger effective area than the projected equivalent area. This contrasts a previous theory by Newman [36] that predicted that cycloturbines could achieve higher performance by splitting the expansion of the flow across the upstream and downstream portions of the rotor.

Acknowledgments

We thank the U.S. Department of Defense for the National Defense Science and Engineering Fellowship for enabling this work. Moreover, we thank Casey Fagley, Thomas McLaughlin, Angela Suplisson, and Neal Barlow at the U.S. Air Force Academy for introducing the problem of blade pitch kinematics on cyclorotors.

References

[1] Benedict, M., Lakshminarayan, V., Pino, J., and Chopra, I., "Fundamental Understanding of the Physics of a Small-Scale Vertical Axis Wind Turbine with Dynamic Blade Pitching: An Experimental and Computational Approach," *AIAA/ASME/ASCE/AHS/ASC Structures, Structural Dynamics, and Materials Conference*, AIAA Paper 2013-1553, April 2013.

[2] Dabiri, J., "Potential Order-of-Magnitude Enhancement of Wind Farm Power Density via Counter-Rotating Vertical-Axis Wind Farm Turbine Arrays," *Journal of Renewable and Sustainable Energy*, Vol. 3, July 2011, Paper 043104.

[3] Kirke, B. K., "Evaluation of Self-Starting Vertical Axis Wind Turbines for Stand-Alone Applications," Ph.D. Thesis, School of Engineering, Griffith Univ., Gold Coast Campus, Southport, QLD, Australia, April 1998.

[4] Borg, M., Shires, A., and Collu, M., "Offshore Floating Vertical Axis Wind Turbines, Dynamic Mode Model State of the Art. Part I: Aerodynamics," *Renewable and Sustainable Energy Reviews*, Vol. 39, Aug. 2014, pp. 1214–1225. doi:10.1016/j.rser.2014.07.096

[5] Borg, M., Collu, M., and Kolios, A., "Offshore Floating Vertical Axis Wind Turbines, Dynamics Modelling State of the Art. Part II: Mooring Line and Structural Dynamics," *Renewable and Sustainable Energy Reviews*, Vol. 39, July 2014, pp. 1226–1234. doi:10.1016/j.rser.2014.07.122

[6] Sasson, B., and Greenblatt, D., "Effect of Leading-Edge Slot Blowing on a Vertical Axis Wind Turbine," *AIAA Journal*, Vol. 49, No. 9, 2011, pp. 1932–1942. doi:10.2514/1.J050851

[7] Greenblatt, D., Ben-Harav, A., and Mueller-Wahl, H., "Dynamic Stall Control on a Vertical-Axis Wind Turbine Using Plasma Actuators," *AIAA Journal*, Vol. 52, No. 2, 2014, pp. 456–462. doi:10.2514/1.J052776

[8] Tescione, G., Ferreira, C., and VanBussel, G., "Analysis of a Free Vortex Wake Model for the Study of the Rotor and Near Wake Flow of a Vertical Axis Wind Turbine," *Renewable Energy*, Vol. 87, Nov. 2016, pp. 552–563. doi:10.1016/j.renene.2015.10.002

[9] Shi, L., Riziotis, V., Voutsinas, S., and Wang, J., "A Consistent Vortex Model for the Aerodynamic Analysis of Vertical Axis Wind Turbines,"

Journal of Wind Engineering and Industrial Aerodynamics, Vol. 135, Dec. 2014, pp. 57–69.

[10] Islam, M., Ting, D., and Fartaj, A., "Aerodynamic Models for Darrieus-Type Straight-Bladed Vertical Axis Wind Turbines," *Journal of Renewable and Sustainable Energy*, Vol. 12, No. 4, May 2008, pp. 1087–1109. doi:10.1016/j.rser.2006.10.023; also Noll, R. B., Ham, N. D., and Peraire, J., "Analytical Evaluation of the Aerodynamic Performance of a High-Reliability Vertical-Axis Wind Turbine," *Proceedings of AWEA National Conference*, 1980.

[11] Anderson, J., Brulle, R., Birchfield, E., and Duwe, W., "McDonnell 40 Kw Giromill Wind System, Phase I: Design and Analysis, Volume I: Executive Summary," McDonnell Aircraft Company TR RFP-3032/1, St. Louis, MO, 1979.

[12] Strickland, J., Webster, B., and Nguyen, T., "A Vortex Model of the Darrieus Turbine: An Analytical and Experimental Study," *Journal of Fluids Engineering*, Vol. 101, No. 4, Dec. 1979, pp. 500–505. doi:10.1115/1.3449018

[13] Schatzle, P., Klimas, P., and Spahr, H., "Aerodynamic Interference Between Two Darrieus Wind Turbines," Sandia National Labs. TR, SAND81-0896, Albuquerque, NM, April 1981.

[14] Vandenberghe, D., and Dick, E., "Optimum Pitch Control for Vertical Axis Wind Turbines," *Wind Engineering*, Vol. 11, No. 5, 1987, pp. 237–247.

[15] Chowdhury, A., Akimoto, H., and Hara, Y., "Comparative CFD Analysis of Vertical Axis Wind Turbine in Upright and Tilted Configuration," *Renewable Energy*, Vol. 85, July 2015, pp. 327–337.

[16] Li, C., Zhu, S., Xu, Y., and Xiao, Y., "2.5D Larger Eddy Simulation of Vertical Axis Wind Turbine in Consideration of High Angle of Attack Flow," *Journal of Renewable Energy*, Vol. 51, Oct. 2013, pp. 317–330. doi:10.1016/j.renene.2012.09.011

[17] Howell, R., Qin, N., Edwards, J., and Durrani, N., "Wind Tunnel and Numerical Study of a Small Vertical Axis Wind Turbine," *Journal of Renewable Energy*, Vol. 35, No. 2, 2010, pp. 412–422. doi:10.1016/j.renene.2009.07.025

[18] Zuijlen, C. F. V., Bijl, H., Bussel, G. V., and Kuik, G. V., "Simulating Dynamic Stall in a Two-Dimensional Vertical-Axis Wind Turbine: Verification and Validation with Particle Image Velocimetry Data," *Wind Energy*, Vol. 13, No. 1, May 2010, pp. 1–17. doi:10.1002/we.v13:1

[19] Templin, R., "Aerodynamic Performance Theory for the NRC Certical-Axis Wind Turbine," National Research Council Lab. TR LTF-LA-190, Ottawa, Ontario, June 1974.

[20] Paraschivoiu, I., "Aerodynamic Loads and Performance of the Darrieus Rotor," *Journal of Energy*, Vol. 6, No. 2, 1982.

[21] Paraschivoiu, I., and Delclaux, F., "Double Multiple Streamtube Model with Recent Improvements," *Journal of Energy*, Vol. 7, No. 3, May–June 1983.

[22] Wilson, R., and Lissaman, P., "Applied Aerodynamics of Wind Power Machines," Oregon State Univ. Tech. Rept. GI-418340, Corvallis OR, July 1974.

[23] Read, S., and Sharpe, D., "An Extended Multiple Streamtube Model for Darrieus Wind Turbines," *2nd DOE/NASA Wind Turbines Dynamics Workshop*, NASA Paper CP-2186, Cleveland, OH, Feb. 1981, pp. 19–25.

[24] Soraghan, C., Leithead, W., Yue, H., and Feuchtwang, J., "Double Multiple Streamtube Model for Variable Pitch Vertical Axis Wind Turbines," *AIAA Applied Aerodynamics Conference*, AIAA Paper 2013-2802, June 2013.

[25] Larsen, J., Nielsen, S., and Krenk, S., "Dynamic Stall Model for Wind Turbine Airfoils," *Journal of Fluids and Structures*, Vol. 23, 2007, pp. 959–982.

[26] Dyachuk, E., Goude, A., and Bernhoff, H., "Dynamic Stall Modeling for the Conditions of Vertical Axis Wind Turbines," *AIAA Journal*, Vol. 52, No. 1, Jan. 2014, pp. 72–81. doi:10.2514/1.J052633

[27] Wilson, R., *Wind Turbine Technology*, ASME Press, Fairfield, NJ, 2009, pp. 281–350.

[28] Benedict, M., "Fundamental Understanding of the Cycloidal-Rotor Concept for Micro Air Vehicle Applications," Ph.D. Thesis, Univ. of Maryland, College Park, MD, 2010.

[29] Rathi, D., "Performance Prediction and Dynamic Model Analysis of Vertical Axis Wind Turbine Blades with Aerodynamically Varied Blade Pitch," M.S. Thesis, North Carolina State Univ., Raleigh, NC, 2012.

[30] Asher, I., Drela, M., and Peraire, J., "A Low Order Model for Vertical Axis Wind Turbines," *AIAA Applied Aerodynamics Conference*, AIAA Paper 2010-4401, June–July 2010.

[31] Migliore, P., Wolfe, W., and Fanucci, J., "Flow Curvature Effects on Darrieus Turbine Blade Aerodynamics," *Journal of Energy*, Vol. 4, No. 2, 1980, pp. 49–55. doi:10.2514/3.62459

[32] Critzos, C., and Heyson, H., "Aerodynamic Characteristics of NACA 0012 Airfoil Section at Angles of Attack from 0 to 180," NACA TR 3361, 1955.

[33] Vandenberghe, D., and Dick, E., "A Theoretical and Experimental Investigation into the Straight Bladed Vertical Axis Wind Turbine with Second Order Harmonic Pitch Control," *Wind Engineering*, Vol. 10, No. 3, 1986, pp. 122–138.

[34] Madsen, H., and Lundgren, K., "The Voith-Schneider Wind Turbine," Inst. of Industrial Constructions and Energy Technology, Aslborg Univ. Centre Tech. Rept. NP-2900722, Denmark, 1980.

[35] Leishman, G., *Principles of Helicopter Aerodynamics*, Cambridge Univ. Press, New York, 2006, pp. 730–731.

[36] Newman, B., "Actuator-Disc Theory for Vertical Axis Wind Turbines," *Journal of Wind Engineering and Industrial Aerodynamics*, Vol. 15, Nos. 1–3, 1983, pp. 347–355. doi:10.1016/0167-6105(83)90204-0

M. Smith
Associate Editor